LRP 440/91 October 1991

PARASITIC ANTENNA LOADING MEASUREMENTS AND A COMPARISON BETWEEN SHIELDED AND UNSHIELDED ANTENNA EXCITATION DURING ALFVEN WAVE HEATING IN TCA

G.G. Borg and B. Joye

PARASITIC ANTENNA LOADING MEASUREMENTS AND A COMPARISON BETWEEN SHIELDED AND UNSHIELDED ANTENNA EXCITATION DURING ALFVEN WAVE HEATING IN TCA

G.G. BORG* and B. JOYE

Centre de Recherches en Physique des Plasmas
Association EURATOM - Confédération Suisse
Ecole Polytechnique Fédérale de Lausanne
21 Av. des Bains, CH-1007 Lausanne, Switzerland

ABSTRACT

Experimental measurements are presented of the parasitic loading resulting from an RF Langmuir current which flows from an unshielded antenna to the scrape-off layer (SOL) during Alfvén wave heating (AWH) in TCA. The measurements are of relevance to ICRH where RF currents drawn by electrostatic screens lead to parasitic loading and harmonic generation in the SOL. An experimental study of the plasma response to AWH after the installation of screens on the AWH antennas is also presented. The results demonstrate that the fault current and some of the parasitic phenomena observed in the SOL during AWH with unshielded antennas are eliminated by screens. The plasma bulk response however is dominated by a large density rise which is unaffected by screens. The implications of these results for AWH are also discussed.

* Present Address.

Australian National University, Plasma Research Laboratory, Research School of Physical Sciences. Canberra 2601 Australia.

1. INTRODUCTION

Despite the general acceptance of electrostatic screens in ICRH (Ion Cyclotron Resonance Heating) for the protection of the plasma from the effects of the near fields of the rf antenna, it has always been considered that low voltages at low frequency have made screens unnecessary in Alfvén Wave Heating (AWH) [1]. Despite this, AWH performs rather poorly as a heating method; the plasma response being dominated by a density rise which may be as large as 300% of the target density. It is now known that this density increase arises neither from impurities nor from a change in recycling [2,3]. Although heating of the electrons and less so of the ions has been observed [24,25], the true potential of AWH is limited by, and an important but poorly understood aspect of the physics of AWH is the cause of, the density rise. In addition, an extensive range of phenomena has been observed in the plasma scrape-off layer (SOL); some of which may be related to the bulk plasma response. During AWH, the SOL density is observed to decrease [4], the SOL floating potential and plasma density are perturbed in a way that reflects the Alfvén wave spectrum [5], the antennas charge negatively [1] and draw a large current from the plasma [6] and harmonics have been observed on edge wave fields [7]. The cause of these effects and their effect on the bulk plasma response is not known. Similar phenomena have been studied for many years in ICRH where antennas are routinely shielded and can only be expected to be worse if the antenna is exposed directly to the plasma. In this paper we describe a series of experiments performed in the TCA tokamak in which the sheath effect at the interface between an unshielded antenna and the plasma was studied for evidence of parasitic loading and a comparative study of the static edge and global plasma response to AWH with unshielded and electrostatically shielded antennas was made. In a companion paper [7] we study in more detail the causes of the phenomena observed in the SOL during AWH.

In AWH an array of antennas external to the plasma excites the surface magnetoacoustic wave; the first radial mode of the magnetoacoustic wave at frequency ω lower than the ion cyclotron frequency ω_{ci}. This wave exists at $\omega < \omega_{ci}$ in small tokamaks for poloidal mode numbers different from zero. According to theory the surface wave is excited most efficiently when the main component of the antenna near magnetic field is parallel to the total steady field. As a result, antenna elements in AWH are aligned in the poloidal direction. The surface wave mode converts to the Alfvén wave in

the neighbourhood of surfaces in the plasma where $\omega^2/(k_{||}V_A)^2 = (1 - \omega^2/\omega_{ci}^2)$, the Alfvén wave dispersion relation, is satisfied. In this expression, V_A is the local Alfvén speed and $k_{||}$ is the local parallel wave number. In a tokamak, $k_{||} = (n + m/q)/R$ where q is the safety factor, R is the major radius and n and m are respectively the toroidal and poloidal mode numbers. If the local electron thermal speed is greater than V_A, the kinetic Alfvén wave (KAW) is excited and propagates toward the plasma centre. If the local electron thermal speed is lower than V_A, the surface electrostatic wave (SEW) is excited which propagates toward the plasma edge. Plasma heating arises in theory by the damping of these waves. Under typical tokamak conditions, the KAW is heavily damped in the plasma interior by electron Landau damping whereas the SEW is damped only slightly in the plasma edge by electron-ion collisions. Despite a large experimental and theoretical effort [8,9,10,11] to study the KAW with excellent agreement demonstrated between theory and experiment, comparatively little is known about the SEW; probably because it is of no interest to useful Alfvén wave heating scenarios.

Experimentally and theoretically, the loading observed in AWH is small; values of 10 to 100 mΩ being typical. In section 2 of this paper we concentrate on experiments performed from which the parasitic power dissipated by the rf Langmuir current flowing from an unshielded antenna to the plasma could be estimated. This currrent will henceforth be referred to as the fault current in analogy with the name given in electronics to that current which flows from a floating transformer secondary to earth during a fault condition. The fault current is the most likely candidate for parasitic loading in rf heating experiments where active elements are exposed directly to the plasma such as in AWH. In ICRH, the voltage induced in the screen by the antenna is large enough at high frequency to cause a variety of parasitic effects in the SOL; some resulting from the high electric fields and some from the fault current. Despite this, no measurement of the power dissipated at the screen-SOL interface by this current has ever been made. In this paper it is shown that the fault current can lead to significant parasitic loading in AWH if antenna excitation ceases to be symmetric (push-pull) and the antenna floating with respect to the torus. The question is important because the choice of antenna elements aligned along the poloidal direction to maximise coupling to the surface wave in AWH, also maximises the surface area of the antenna viewed by plasma along the direction of the toroidal magnetic field; the direction from which the fault current obviously flows.

In section 3 we examine the effects of two types of electrostatic screen on the plasma SOL and global response to AWH. Two types of mechanically identical electrostatic screen were studied. In the first, the screen was floating with respect to the torus and in the second the screen was earthed at the torus. The earthed screen can draw fault current and should shield direct electrostatic coupling from the plasma whereas the floating screen draws little or no fault current and would tend to enhance electrostatic coupling. In both cases however the particle shielding effect and magnetic coupling responsible for Alfvén wave excitation is identical and the fault current drawn by the antenna completely eliminated. This allows us immediately to determine whether a fault current or a direct coupling of the elctric field is of importance in AWH. For example, direct electrostatic coupling of high electric fields in the plasma edge leads to parametric decay instabilities in ICRH [12, 13]. The experiments will also determine what parasitic effects arise from magnetic coupling and are therefore an unavoidable consequence in AWH. In this paper we concentrate on the static edge and global plasma response to AWH with and without screens.

These experiments were motivated by results from the TORTUS tokamak [14] which indicated that the density rise may be eliminated by electrostatic screens. They performed two experiments. In the first, an unshielded Cu loop antenna, similar in structure to a single one of the six elements which comprise a single TCA antenna, was excited at a given power and in the second, the same antenna was excited at a similar power after installation of a TiN coated earthed electrostatic screen made of aluminium. In the first case a large density rise ($\approx$ 30% of the starting density for $\approx$8 kW into plasma) was observed which was completely elimimated in the second. We repeated the TORTUS experiment at higher power in an attempt to eliminate the density rise seen in TCA. Elimination of the density rise would allow the heating effects in AWH to be much more easily observable.

2. PARASITIC LOADING MEASUREMENTS

Experiments were performed to determine the parasitic power deposited at the antenna-plasma interface by the fault current. The fault current is driven by the voltage between the plasma and the antenna along the length of the antenna. The antenna therefore behaves like a distributed Langmuir probe.

In TCA (see Fig. 8) there are four pairs of top and bottom antennas distributed at 90^0 intervals around the machine. Each antenna consists of six parallel bars which are floating with respect to the torus [1]. The antennas were excited at 2 MHz and were designed for symmetric excitation. The fault current was measured by subtracting the signals obtained from two wideband Rogowski coils mounted on the input and output terminals of one of the three bar pairs forming the antenna. Since the fault current has a detailed high frequency structure which bears on the parasitic power it gives rise to, care had to be taken to preserve this structure in the measurement and to eliminate unwanted rf pickup. For this purpose, a passive electronic circuit based on a hybrid combiner [15] was constructed in which the amplitude and phase of the input current signals could be adjusted to compensate the slight difference in the Rogowski characteristics and to perfectly cancel the observed signal in the absence of plasma. The bandwidth of the total system was about 10 MHz. A diagram of the experimental arrangement is shown in Fig.1.

The resolution of the measurement is limited nonetheless by electrostatic pickup. Electrostatic pickup was estimated by comparing the output signal from the Rogowskis for open-circuit excitation of the antenna with a certain antenna voltage. This signal, which is ideally zero, was observed to be about 2% of that detected with the antenna circuit closed so that current could flow with the same voltage across its terminals. In addition, the signal at the output of the subtraction electronics could be adjusted to a level much lower than this pickup level for a shot with rf but without plasma where the fault current is zero. In this case the pickup as well as the imbalance in the two signal channels is adjusted to zero at the same time. The real error in the fault current measurement is therefore due to the residual pickup introduced during plasma when the relative amplitudes of the two terminal voltages of the antenna are different compared with the case of no plasma. The error in the fault current is therefore much lower than 2% of the circulating current.

Under symmetric excitation, the fault current measured consists of the difference of two currents flowing simultaneously during a given half-cycle of the antenna voltage. A current consisting mainly of electrons flows from the plasma to points on the antenna at positive potential with respect to the plasma and a current consisting of ions flows from the plasma to points on the antenna at negative potential with respect to the plasma. Since the configuration is necessarily symmetric the measured fault current must have a frequency twice that of the antenna terminal voltage. Part of this fault current flows through the antenna terminals and is measured, the rest flows between the antenna and the plasma and is not detected by the Rogowski coils. The relative magnitudes of each current depend on the respective impedances presented by the two paths to the plasma. The measured fault current in this case is therefore smaller than the actual total fault current reaching the antenna from the plasma. In fact, if the current arriving at any given point on the antenna had a sinusoidal waveform with no distortion the fault current detected at the antenna terminals would not be observable at all. If on the other hand, the antenna is excited asymmetrically with one terminal at rf ground and the other at rf potential, the fault current is unidirectional at each point along the antenna on every half-cycle. As a result, the measured fault current has the same frequency as the antenna terminal voltage and, since all this current flows through the antenna terminals and is measured by the Rogowski coils, it should be larger than that detected in the case of symmetric excitation. These ideas are demonstrated schematically in Fig. 1 where current paths are indicated by the arrows. Note from the figure that, since the RF generator is symmetric, inductances whose parallel vacuum value ($\approx$ 170 nH) is equal to that of the antenna have to be inserted in series with each of the elements of the antenna in order to provide floating asymmetric excitation

The validity of these ideas is confirmed by the experimental traces of the fault current measured during asymmetric and symmetric excitation. The raw signals are shown in Fig. 2a for similar values of the circulating antenna current in each case. The signals are the derivatives of the total antenna circulating currents and the fault currents. The traces for asymmetric excitation are shown in the left column and symmetric excitation in the right column. The symmetric fault currents were obtained for m = 0 and m = 1 and are shown on the right in the second and third rows. Note that the amplitudes of these fault currents are similar in each case, but that there is a slight difference in their temporal structures probably due to a slight asymmetry in excitation. We note in particular the fact that the fault current for symmetric excitation has twice the frequency of that for asymmetric excitation.

For asymmetric excitation, the minimum and maximum RF power delivered to the antenna-plasma interface by the fault current can be estimated. To see this, we show in Fig. 2b a full set of asymmetric data taken during the rf pulse for one shot. From top to bottom are shown the raw and integrated fault currents I_f, antenna terminal voltage V_{int}, circulating current entering the active terminal I_{int}, and circulating current leaving the terminal at rf earth I_{ext}. The voltage on the terminal at rf earth V_{ext}, was negligible with respect to V_{int}. Note that the fault current is quite large compared with the circulating currents and that it is in phase with the driving voltage.

In Fig 2c the rms amplitude of the fault current is plotted versus V_{int}. The curve has a distinct knee at a voltage approximately equal to the plasma edge electron temperature, above which it is essentially offset linear.

Since the fault current is observed to be in phase with the antenna voltage and since it is reasonable to assume that the fault current at any point along the antenna is a monotonically increasing function of voltage, the minimum power deposited by the fault current must result when the fault current is delivered uniformly along the length of the antenna. We assume in addition that the fault current delivered by each of the three antenna element pairs are similar and that the antenna-plasma resistance is sufficiently large in comparison to the antenna inductance along the element in contact with the plasma that the antenna voltage amplitude varies linearly along the antenna. The effective voltage driving the fault current is therefore the average of the antenna terminal voltages. Provided we neglect the voltage, V_{ext}, the minimum power is given by,

$$P_{min} = \frac{1}{2}\langle I_f V_{int}\rangle.$$

An effective antenna resistance can be defined with respect to the circulating antenna current ($I_{ant} = (I_{int} + I_{ext})/2$) as follows,

$$R_{min} = 2P_{min}/I_{ant}^2 \qquad (1)$$

Similarly the maximum power can be defined as that which results when all the fault current flows from the point on the antenna at highest rf voltage in contact with plasma. This point is that which is closest along the antenna to the terminal at V_{int}; it is marked with a P in Fig. 1. The voltage, V_P, is clearly not measured in the experiments but can

be estimated from knowledge of the inductance L_{int} in the radial feeder element between P and the point at potential V_{int} by

$$V_P = V_{int} - L_{int}\frac{dI_{int}}{dt}.$$

The inductance L_{int} was estimated by in situ measurements to be 35 nH. The maximum fault current power is given by

$$P_{max} = \langle I_f V_P \rangle$$

from which a corresponding parasitic loading can be estimated from,

$$R_{max} = 2P_{max}/I_{ant}^2 \qquad (2)$$

The total power delivered from the antenna to the plasma for asymmetric excitation was calculated from the difference between the antenna loadings for plasma and vacuum based on the power entering the antenna matching network and a measurement of the circulating current in the antenna. This is the conventional Alfvén loading measurement and includes both the real Alfvén loading as well as all parasitic loadings. Calculations were made of the parasitic loadings of equations (1) and (2) and compared with the total loading measurements. The results are shown in Fig 3a as a function of circulating antenna current where the points are the total loading and the bars cover the range from R_{min} to R_{max}.

We note that the loading is a decreasing function of increasing antenna current. This result is possibly of relevance to previous total loading measurements in AWH [1] and ICRH [16]. It is a general property of the loading regardless of excitation mode numbers (n,m). This non-linearity can be understood as follows. Consider the following definition of the fault current loading;

$$R_f^* = I_f(\text{rms}) * V_f(\text{rms})/(2\, I_{ant}^2)$$

where I_f(rms) and V_f(rms) come from Fig. 2c. For the values of antenna current in Fig. 3a the R_f^* values so obtained lie within the bars of the I_f loading extrema. This indicates that the non-linearity in the loading characteristic is mainly due to the offset linear nature

of the fault current characteristic in Fig. 3c and is not due to a variation in the phase of the fault current with respect to its driving voltage or of the edge plasma parameters. We conclude that, for asymmetric antenna excitation of unshielded antennas in AWH, practically all loading in the low power range (up to 20 kW) is fault current loading.

We now estimate an upper limit to the fault current loading for the case of symmetric excitation of an antenna floating with respect to the torus; the case of general interest in AWH. In Fig. 3b, we show the total loading for symmetric excitation of a single antenna versus circulating antenna current. Comparison with Fig 3a indicates that the total loading is reduced by about a factor of 5 for the same antenna current compared with the same antenna under asymmetric excitation. This result highlights the importance of symmetric excitation of unshielded antennas in AWH. The decrease in loading must be attributable to a decrease in fault current loading since the Alfvén portion arises from magnetic coupling and cannot be dependent on the symmetry of antenna excitation. The loading, however, is still non-linear in agreement with previous observations.

To provide a crude upper estimate of the fault current loading for symmetric excitation we proceed as follows. If we assume that the voltage at point P in Fig. 1 is $V_{int}/2$ and at point Q is $-V_{int}/2$, then we may conclude that the circulating current in the antenna is given by,

$$V_{int} = L_{PQ}\frac{dI_{ant}}{dt} \qquad (3)$$

where L_{PQ} is the portion of antenna inductance between P and Q. In practice V_{int} and I_f can be obtained from a shot in which the antenna was excited asymmetrically. The maximum power dissipated by the fault current occurs when the fault current flows uniquely from the points P and Q. For asymmetric excitation we saw that a voltage $V_{int}/2$ at the antenna centre drives a fault current I_f along the length PQ of the antenna exposed to the plasma. In the present case $V_{int}/2$ has only half the length of antenna to drive the fault current so that each side of the antenna contributes in equal amplitude but opposite phase, $I_f/2$ at voltage $V_{int}/2$. Each side of the antenna will indeed drive this current provided we assume similar plasma conditions and neglect the effects of antenna dc self-polarisation [1] which are different for symmetric and asymmetric excitation. The antenna dc self-polarisation arises when fault current flows because the dc fault current

must be zero if the antennas are floating. The total simulated fault current that would be seen at the antenna terminals by the Rogowskis has been calculated in Fig. 2a for shot 36616 (an asymmetric excitation case). In this case V_{int} is such that I_{ant} from equation (3) has a similar value to that shown in the right hand column of Fig. 2a. The derivatives of the calculated I_{ant}, the experimental $I_f/2$ and the calculated symmetric fault current are shown from top to bottom in the left hand column of Fig. 2a.

Clearly the detailed structure of the simulated current does not correspond at all to the experimental cases shown; a result which is not too surprising considering the physical effects neglected in its calculation and the fact that two large signals of detailed time structure have been subtracted. The amplitude and the phase with respect to I_{ant} however are not too bad, giving us confidence that the fault current loading upper limits estimated from the asymmetric data used for Fig. 3a are approximately correct. The points defining this loading upper limit are plotted as open circles in Fig. 3b. The density at which the total loading measurements were made was just below the threshold of the (1,1) DAW. The rectangle gives an estimate of the error in the calculation however it has little meaning in this case since the potential minimum loading values are now much lower than the maximum values. An estimate of the minimum loading would correspond to the case where $V_{int}/2$ lies at the point halfway between the centre of the antenna and P and $-V_{int}/2$ between the centre of the antenna and Q with $I_f/2$ flowing uniformly between the centre point and P and similarly between the centre point and Q. From equation (3) this will double I_{ant} for the same fault current power leading to a minimum loading equal to 0.25 of the maximum loading.

Despite the clear interpretation of the results for asymmetric excitation, confirmed by the large decrease in loading witnessed for symmetric excitation, it is not possible to state what fraction of the symmetric antenna loading, if any at all, is Alfvén loading. In addition, no measurements were made of the fault current on the central bar pairs of the antenna. If these bars collect a much smaller fault current than the outer bars then the fault current loading measurements presented here have to be multiplied by 2/3. This is quite possible since the fault current is expected to flow along field lines and may be obstructed by the outer elements. Despite this, the fault currents observed on the outer bars, as described, are similar for antennas separated toroidally by 180^0 for similar levels of excitation.

To make the estimate of the fault current loading more accurate requires more accurate knowledge of the detailed structure of the symmetrically excited fault currents of Fig. 2b. This could proceed by simulating the fault current for various plasma conditions and antenna dc self-polarisations. For symmetric excitation the dc self-polarisation is large enough compared with the voltages at points P and Q that it cannot be neglected in the modelling. This is especially the case if only a single antenna or antenna pair is being excited. When all four antenna pairs are excited the dc self-polarisation is much lower [1].

According to the experimental symmetric fault current traces in Fig. 2a the m = 0 fault current is more symmetric than the m = 1 fault current loading. It is as if m = 1 excitation is more asymmetrised than m = 0 excitation. In TCA under symmetric excitation, the antenna terminal voltages do tend to asymmetrise; probably as a result of toroidal geometry, confirming the asymmetrised m = 1 fault current trace in Fig. 2a obtained during symmetric excitation. This asymmetry is not too surprising since the coupling between top and bottom antennas, even in a vacuum in TCA, is large and opposite for m = 1 and m = 0 excitation. This means that the fault current loading is not strictly non-coherent loading as previously assumed [1]. According to the above discussion we should expect a larger parasitic loading for m = 1 than for m = 0. Interestingly, the total loading for m = 1 is experimentally always at least three times larger than for m = 0 [1]. This result agrees qualitatively with the theory of coupling to the Alfvén wave by excitation of the surface wave by an external antenna as previously mentioned. We now conclude that a portion of the difference between m = 1 and m = 0 loading must be parasitic at low power. This conclusion is based on the detailed short timescale structure of the fault current.

One can pursue the question of non-coherence of the fault current loading still further and consider the long timescale structure as the fault current evolves with changing plasma density. The m = 1 total loading traces at high power in AWH [1] have considerable reproducible structure as a function of density which depends on the toroidal mode number n. The detail consists of large peaks at the Discrete Alfvén waves (DAWs) and continua of featureless loading in between. This structure is indicative of the Alfvén spectrum [1]. The fault current on the other hand is driven by the voltage along the antenna. This voltage is rather insensitive to the Alfven spectrum and the fault current should be even more so since, from Fig. 2c, it is a less than linear function of voltage. Experimentally the fault current structure is indeed quite featureless and independent of

the Alfvén spectrum. This is not necessarily an evident experimental result. The fault current should, for example, be influenced by rf oscillations in the plasma potential during AWH. These oscillations, typically 10 - 100 V-pk in amplitude, follow the Alfvén spectrum and are largest during DAWs. A modulation of the fault current by the rf plasma potential has not been clearly observed in the experiments. At high power however, changes in the fault current during passages of the DAW are clearly observed, probably due to the effects of the high power rf on the SOL dc parameters.

In Fig. 3c, signal traces are shown of the antenna current, total antenna loading, the derivatives of the fundamental $I_f(0)$ and first harmonic $I_f(1)$ of the fault current and a typical fundamental wavefield trace observed during excitation of antenna 3. These results were taken at 2.5 MHz during the passage of the (2,1) DAW. The main point to notice is that a portion of the total loading at $t > 0.13$ s is clearly due to the DAW and probably the ARL which enters the plasma. This increase in loading cannot be explained by the fault current since there is but minimal influence of the DAW evident in the fault current traces. The results in Figs. 2 and 3 were taken at 2 MHz where the density of the (2,1) DAW could not be reached in D_2 under normal operating conditions in TCA.

Since the fault current is always in phase with the driving voltage, the power dissipated by the fault current and hence the fault current loading must also have no structure. From these arguments, we are convinced that the total loading traces observed must contain some real Alfvén wave loading; even in the continua, but that the zero base line of Alfvén loading may be higher than that previously estimated [1] by the $m = 0$ loading.

From Figs. 2c and 3b, the fault current parasitic loading is inherently a decreasing function of increasing antenna current. This property of the fault current loading permits us to demonstrate that the measured antenna loading is not totally due to the fault current. Experiments had been previously performed in TCA in which various types of side screen were installed on one top and bottom pair of antennas [17]. Measurements of the nonlinear loading compared with the case of no screens for two densities and for $m = 1$ excitation are shown in Fig. 4. Four types of screens were tested. 1) Solid metallic side screens similar to those to be described later in this paper, entirely blocked the view along field lines. 2) Slit side screens similar in construction to the solid side screens but with slots to prevent attenuation of the wavefield. 3) Solid quartz side screens of similar construction to the solid metallic screens. 4) A set of side skirts shielding the antenna feeders but not the poloidal bars along field lines. Unfortunately

the fault current was not measured in these experiments, however the total loading measured for the case of solid metallic and ceramic side screens and slit side screens is a flat function of antenna power, indicating that the fault current parasitic loading had been eliminated in these cases.

The parasitic loading estimates presented indicate that care has to be taken in the design of antennas for AWH. This is especially the case in low power experiments where the results presented are directly applicable and experiments where asymmetric antenna excitation is involved. Asymmetrisation of the antennas during symmetric excitation will also enhance the parasitic loading due to the fault current. The results also emphasise the importance of minimisation of antenna inductance if the antennas are left unshielded, since the Alfvén portion of the loading arises by wave excitation due to the antenna current and the fault current arises from the antenna voltage. It is also to be expected that the fault current will be larger if the antennas are earthed at the vessel than if they are floating, since the self-polarisation of a floating antenna tends to decrease the electron component of the fault current. Despite the fact that traditionally the antennaas in TCA have been unshielded, each antenna consists of six bars fed symmetrically and floating with respect to the torus. According to the present discussion, this low inductance design has permitted the clear observation of Alfvén wave loading even at low power.

When the DAW is not excited, it is very difficult to distinguish Alfvén from parasitic loading. Power dissipation by the fault current occurs at the antenna-SOL interface and, as we shall see, has no observable effect on the plasma global response, even at high power. In AWH, the plasma response is not significantly perturbed by impurities that may result from the fault current. In addition, the fault current is not the only effect at play in the SOL. Direct measurement is the only way of detecting its presence.

3. ELECTROSTATIC SCREEN DESIGN AND EXPERIMENTAL LAYOUT

Electrostatic screens for a poloidal loop antenna, such as that used for AWH in TCA, generally consist of a group of earthed parallel strip blades aligned along the total steady magnetic field. The function of screens is to prevent particle and current flow between the plasma and the antenna, to form a capacitive divider to divide the potential of the antenna exposed to the plasma and to short out the component of the near electric field along the total steady field ($E_{||}$). If in addition, both ends of the blades are earthed, an image current circulates in the blades and earth which cancels the component of antenna current parallel to the blades. This results in the elimination of waves with finite $E_{||}$ which may be launched by components of the antenna current parallel to the total steady field. At the same time screens must reduce as little as possible the near magnetic field of the antenna necessary for wave coupling. The capacitive divider function is completely suppressed if the blades are floating so high electric fields appear in the SOL, but fault current to the screen is eliminated and the cancellation of $E_{||}$ still occurs.

A test circuit was constructed to examine the properties of electrostatic screens before a final design and experimental proposal for screens was made. The circuit, shown in Fig. 5a, consisted of a single element linear antenna and an electric probe (Fig. 5b). The plasma SOL would normally be around the position of the probe. Two test screens were examined. The first consisted simply of a flat plate of aluminium which could be either earthed to the back plane or left floating. A second version of the test screen was tested in which the ends in the toroidal direction (along the dipole axis of the antenna) were curled back away from the plasma. Curling the blades also gives protection against interaction with particles flowing along field lines. The main electric field component responsible for parasitic plasma coupling is $E_{||}$. The direct field component of $E_{||}$ gives rise to particle acceleration along field lines. Fig. 6 shows a plot of measurements made of $E_{||}$ with and without test screens. Although introduction of screens significantly reduces $E_{||}$ along the screen, the magnitude of $E_{||}$ at the ends of the flat screen increases to about its screenless value if the end is sharp. Curling the ends of the screen away from the plasma reduces $E_{||}$ more uniformly.

The screens used in the AWH experiments are shown schematically in Fig 7. Two types of screen were constructed each consisting of 11 curved blades, 265 mm to 410 mm in total length, approximately 40 mm wide, 0.5 mm thick and separated by 5 mm. In the first, the blades were earthed to the torus at one end by stainless steel supporting poles. In the second the poles were insulated by ceramic stand-offs, and were floating. Due to the complicated three dimensional geometry of the antennas in TCA, the screen blades were aligned along the toroidal field and not along the total steady field in order to make fabrication feasible. As a result, in the case of the earthed screen, nothing is gained by earthing the blades at both ends since the antenna has no toroidally directed current elements; in fact, it gives a measure of protection against radial forces induced in the screens during plasma disruption. This means that waves that may be launched by the small component of antenna current parallel to the poloidal field at finite plasma current are not eliminated by these screens. As an example, in ICRH in JET [18], it has been shown that the small antenna current component parallel to the poloidal field couples to the evanescent Slow Wave (SW) which causes observable parasitic effects and lower heating efficiency compared with experiments in which the screen elements were aligned parallel to the total field and the SW was eliminated. The only wave known to exist below the ion cyclotron frequency which is excited directly by parallel current elements is the guided Alfvén wave (or SEW) [15]. For experimental conditions similar to ours, however, it has been shown [19] that this wave is more efficiently excited by the parallel component of wave magnetic field at finite frequency and therefore cannot be eliminated by screens. Examination of such effects is in any case best performed with a rotatable antenna so that the orientation of the antenna current elements can be varied from shot to shot. In addition, there is also a small component of antenna near $E_{||}$ due to poloidal field. The separate effect of this field was not identified in the JET experiments, however we assume that if it is important, the biggest effect has already been achieved by eliminating its toroidal component. In fact, in ICRH, a large improvement in general performance is already obtained between the cases of no screens and simple toroidal screens. It is only to be expected that, at the high power levels and higher frequencies of ICRH compared with AWH, one can make an additional gain by using parallel screens.

In each case, earthed side screens on each side of the antenna were incorporated to completely obstruct particle flow along field lines. This precaution appeared necessary because the plasma density in the SOL behind the antenna radius is as high as $1\text{-}5\ .10^{18}\ m^{-3}$ with electron temperatures around 10 eV [4]. The side screens were far enough from the antenna so as not to interfere with antenna wave coupling more than the

blades.The screens were made of the same material as the antennas, nonmagnetic stainless steel, in order to avoid complications in the interpretation of plasma response as a result of impurities when comparing with unshielded antennas. The choice of a low resistivity screen to improve efficiency was not a consideration since the rf generator, AFCO [20], could provide over 100 kW per antenna. In these experiments, this power level is more than enough to recognise the plasma response in the presence of screens. In high power experiments however, or where generator output power is limited, care does have to be exercised in the choice of screen material [21].

An important property of the screens is the amount that they permit the near magnetic field of the antenna to penetrate through to the plasma. The magnetic field transparency of the screens was measured at almost 100%. This a result of the fact that in designing the screens, care was taken to ensure that the near magnetic field of the antenna was nowhere normal to the screen elements [22]. Further aids are to keep the blades thin and to maximise their number in order to decrease the inductance along paths where eddy currents flow in the screen elements. We conclude that any decrease in coupling to the plasma must be a result of the decrease in near-antenna-density as a result of the screens. In practice, a decrease in the edge plasma density leads to a decrease in the Alfvén wave loading. In these experiments, at the highest powers obtained, the antenna loading decreased by about a factor of two. Bench tests of $E_{||}$ elimination were not performed due to the complicated three dimensional geometry of the screens.

Typically the RF voltage expected between the antenna terminals and the torus is about 1 kV peak. In TCA the gas particle mean free path is too long for gas breakdown to occur in the low MHz range. Breakdown must therefore occur by secondary electron emission from the antenna and screen material; a phenomenon known as multipacting [23]. Multipacting breakdown occurs when the time taken for an electron to travel the distance between two electrodes is equal to half the period of the RF voltage. For breakdown along field lines the minimum cutoff frequency for multipacting between two parallel plate electrodes is given by $f_{min} \approx 80/d$ MHz, where d is in cm. As a result, the antenna could be separated from the screen by *at most* 40 cm along field lines. For breakdown between a thin antenna bar and the screen this distance is even larger since the electric field at the antenna is higher for a given potential difference between the antenna and the screen than for the case of parallel plates. Across field lines, breakdown is not expected because the electron Larmor radius is much smaller than the distance

between screen and antenna. These conditions make breakdown inside the vessel practically impossible below the ion cyclotron frequency. No sign of breakdown was ever observed during the experiments.

The experimental arrangement is shown in Fig. 8. A pair of such screens were constructed for top and bottom antenna pair (1,5) in which the blades were earthed and a second pair for (2,6) in which the blades were floating. Antenna pairs (3,7) and (4,8) were left unshielded.

4. EXPERIMENTAL RESULTS WITH SCREENS

In this section we consider the prior conjecture that one of the benefits of screens in AWH is to eliminate the density rise [14]. If we assume that this hypothesis is correct and that the density rise does not result from impurity release at the antenna or a change in recycling, then parasitic coupling to edge waves or the near fields of the antenna themselves must cause a change in confinement in the plasma edge.

The typical plasma condition employed was $I_p \sim 120$ kA, $B_T = 1.5$ T and electron density ~1-3 x 10^{19} m^{-3}. Under these conditions the central electron temperature was about 800 eV and ion temperature, 300 eV. In section 4.1 we present results which show how the screens influence the static edge plasma response to AWH and in section 4.2 we consider the bulk plasma response.

4.1 The Effects of Electrostatic Screens on the Static Edge Plasma Response to AWH.

In Fig. 9 we show the response of several edge plasma parameters to excitation of unshielded antenna pair (3,7) (Fig. 9a) and shielded antenna pair (1,5) (Fig. 9b) with a similar antenna current. From top to bottom, are the dc self-polarisation V_{pol} for the excited antenna, the probe floating potential, V_{fl}, measured on unexcited unshielded antenna 4 and the ion saturation current, J_{sat}, measured after applying ≈150 V negative potential to antenna 4. In the bottom frame we show a typical antenna current for each case. The main point to note is that for the most part screens eliminate the parasitic phenomenon observed, leaving the antenna substantially unpolarised and the SOL dc properties unaffected by AWH. In addition, no difference in the results was observed between shielded pair (1,5) in which the blades were earthed and shielded pair (2,6)

in which the blades were floating. This result is not surprising in retrospect because the side limiters, which were earthed for both antenna pairs, probably short the blades to the vessel along field lines.

The experimental arrangement as shown in Fig. 1 was reemployed on earthed shielded antenna 1 and unshielded antenna 3 to measure the fault current for symmetric and asymmetric excitation. The fault current for asymmetric excitation was eliminated by screens to a level lower than the limit of resolution of the detection system; or to a level at least 100 times lower than its value without screens. Consequently, any effect on the plasma SOL as a result of the Langmuir interaction of the fault current must also be eliminated to a similar extent. We conclude that the screens function correctly as particle shields.

The results however conceal a lot of detail that needs pointing out and explanation. Firstly, it is to be expected on theoretical grounds that the antenna dc self-polarisation be independent of the SOL electron density provided this density is not drastically altered during the process of polarisation. Previous experimental results [1] appear to confirm that this is the case. The top frames in Fig. 9 indicate however that screens reduce this polarisation by an order of magnitude. This is consistent with the fact that the fault current is unobservable.

The probe floating potential, V_{fl}, response appears to be affected by the Alfvén spectrum [5] during the passage of the (n,m) = (1,1) DAW. This effect is not entirely eliminated by screens since some evidence of the (n,m) = (1,1) DAW is still observable in the case of (1,5) excitation. Clearly such an effect is not simply due to the fault current since, as shown in Fig. 4, the fault current does not have a temporal response sensitive to the Alfvén spectrum. Just the same, the spectral character of the probe floating potential depends on a physical effect almost eliminated by screens. Several interpretations are possible. Perhaps the observed dc potential is not indicative of the true plasma potential but is due to rectification of the rf plasma floating potential at the probe; in this case antenna 4. Measurements of the rf fault current drawn by an unexcited, unshielded antenna (the passive fault current) indicate that this current has a strong Alfvén spectral dependence with a large resonance at the DAWs. The magnitude of this current however (typically a few amperes) is comparable for excitation by screened and unscreened antennas and would therefore give rise to dc floating potentials of similar amplitude.

The observed signal must therefore be real. The cause of this spectrum dependent change in the probe floating potential is not understood.

Curiously the ion saturation current does not have a very strong spectral dependence in Fig. 9 and it appears as though the fault current itself is reponsible for the difference in the traces. Previous measurements at high power with unshielded antennas [5] confirm that during AWH the edge plasma density decreases at the time rf is applied but that considerable spectral effect can be observed including an edge density increase after a DAW. The rf ion saturation current follows the Alfvén spectrum even at low power. At high powers its magnitude is of the order of the static edge density itself [7] and may explain the spectral dependence observed on the static density at high power in the previous experiments. Since a bias potential of -150 volts is used to draw ion saturation current, the measurement is not expected to be significantly perturbed by the plasma potential.

It should be mentioned that the screens themselves can also draw fault current by transformer action during excitation of the shielded antenna. This current is expected to be smaller than that which flows when the bare antenna is exposed directly to plasma. In addition, identical experimental results are obtained with floating and earthed screens. The elimination of the edge V_{fl} and in particular J_{sat} appears to indicate that the fault current drawn by the screens themselves is lower than that drawn by an unshielded antenna. It is not possible however to establish a direct causal link from the present results.

The results of this section demonstrate that screens function correctly by eliminating the obvious direct effects of the antenna near fields and near-antenna density on the plasma SOL, such as the fault current and, to a degree, the probe dc floating potential and the ion saturation current. However the results are not entirely understood since there is a dramatic influence of the Alfvén wave spectrum. In actual fact, considerable non-linear effects are evident in the SOL such as rf harmonics on J_{sat} and the wave magnetic field which are not influenced by screens [7] at all.

4.2 The Effects of Electrostatic Screens on the Global Plasma Response to AWH

Results for the average plasma parameters are shown in Fig. 10. The top frame in each set with AWH shows the plasma current, $\Lambda = \beta + l_i/2$, the second shows the line averaged density and the soft X-ray flux at two radii (0 and 5.3 cm) and the third shows the AWH power and rms antenna current of one of the antennas in each pair. For the screened antennas, the power measurement is not accurate since the total loading measurement gives values < 10 mΩ at 2 MHz. A similar discharge without AWH is shown in Fig. 10d for reference. A single antenna pair was excited at a time in order to study the effects of AWH either with or without screens.

Comparison of the unshielded antenna case in Fig. 10a with Fig. 10d reveals that AWH produces an immediate density rise at the time rf is applied. The density sweep traverses the Alfvén spectrum and crosses the DAW. The density rise is observed to scale with power and to be dependent on the Alfvén spectrum [2]. After the DAW the density flattens. This discontinuity in the density evolution is accompanied by similar discontinuities in other plasma parameters. Here, discontinuities are also evident in Λ, the loop voltage and the soft X-ray traces. These observations are generic to AWH [3,26].

Comparison of the traces obtained for excitation without screens with those for otherwise identical shots with screens, antenna pairs (1,5) in Fig. 10b and (2,6) in Fig. 10c, reveals very little difference in the response of any of the plasma parameters that cannot be attributed to the difference in antenna power for each case. In particular, the density increase, which is known to be almost entirely responsible in itself for the observed changes in Λ and the soft X-ray flux, has not been significantly reduced by screens. The lower rise in the density resulting from lower power in Figs 10b and 10c leads to a slower sweep of the Alfvén spectrum and hence a slower traversal of the DAW. The discontinuity in the density is even more easily observable in Fig 10b than in Fig. 10a. These results also indicate that neither particle effects near the antenna nor antenna near electric fields play a role in the production of the density rise and hence the global response in AWH. Since recycling and impurity release are antenna near field effects, these results are consistent with the fact that the density rise is due to an rf induced change in confinement.

Recent AWH results indicate that the density rise is the same per unit power before and after boronisation [27]. After boronisation, there is a substantial decrease in impurity levels as measured by the level of soft X-ray emission and by spectroscopic techniques. The plasma is even cleaner during AWH because most of the density increase arises from the filling gas. The results of boronisation thus confirm the original conclusions about recycling and impurities. The soft X-ray emission is a very sensitive measure of the level of impurities. It was observed to decrease by a factor of 100 after boronisation even though the density rise remained essentially unchanged. Clearly, if the density increase in Fig. 10a is not due to impurities then, since the soft X-ray levels in Fig. 10b and 10c are similar, the density rise due to screens in these cases cannot be due to impurities either. This eliminates the improbable hypothesis that screens eliminate the conventional density rise and replace it with an impurity related density rise.

5. RESUME AND CONCLUSION

Measurements have been presented of the parasitic power deposited at the antenna-SOL interface by the rf Langmuir current, termed fault current, which flows between an unshielded antenna and the plasma. These results demonstrate that under symmetric excitation the parasitic power delivered to the antenna-SOL interface by the fault current may be significant, especially if excitation tends to become asymmetric. For asymmetric excitation, the fault current parasitic power is an order of magnitude larger than the Alfvén loading for TCA conditions. This necessitates the need for screens in experiments where asymmetric excitation is employed. The amplitude of the fault current is not correlated with the Alfvén spectrum. Evidence for total loading greater than the fault current loading has been obtained which is linked to the Alfvén spectrum. Previous results [1] indicate that the part of the total loading which is sensitive to the Alfvén spectrum is more dominant at high power.

Results have also been presented of experiments in which electrostatic screens have been installed on the antennas in AWH. It has been observed that screens eliminate to a large extent several dc phenomena occurring in the SOL and completely eliminate the fault current. The underlying physical mechanisms responsible for these phenomena however, are not understood. The reduction of automatic polarisation of an excited antenna can be explained by the elimination of the fault current. Effects such as the reduction of probe floating potential and the reduction in the decrease in edge plasma

density are not explainable solely by the fault current since these phenomena are correlated with the Alfvén spectrum. In addition [7], rf phenomena such as the harmonics observed on SOL wavefield quantities and large rf oscillations in the ion saturation current and the passive fault current, all of which are correlated with the Alfvén spectrum, are not affected by screens.

Despite correct electrostatic and particle shielding by the screens, the plasma response to AWH is not affected. In particular the density rise per unit power has not been observably reduced. It should be noted that this does not mean that screens are not necessary in AWH. AWH at MW power levels as currently used in ICRH could necessitate screens to eliminate edge plasma perturbations in the same way as in ICRH. Until the density rise is eliminated however, AWH will be limited to low powers where screens have no influence on the bulk plasma response.

ACKNOWLEDGEMENTS

The authors would like to acknowledge the work of Mr. Claude Raggi who constructed the Rogowski coils and the screens and Messieurs Michel Ries and Claude Raggi who installed the screens in TCA. The authors would also like to thank Drs J.B.Lister, M.L.Sawley and S.Puri for useful discussions. This work was funded by the Fonds National suisse de la Recherche Scientifique.

REFERENCES

[1] Collins G.A., Hofmann F., Joye B. et al. Phys. Fluids **29** p. 2260 (1986)

[2] Collins G.A., Joye B., Lister J.B. and Moret J.-M. Proc. of the 12th European Conf. on Contr. Fus. and Plas. Phys., Budapest, Vol. 9, p. 248 (1985)

[3] Besson G., Borg G.G., Lister J.B. et. al. Proc. of the 17th European Conf. on Contr. Fus. and Plas. Phys. Amsterdam, Vol. 14, p 1175 (1990)

[4]. Hofmann F., Hollenstein Ch., Joye B., et al. J. Nuc. Mat. **121** p. 22 (1984)

[5] Martin Y. and Hollenstein Ch. J. Nuc. Mat. 162-164 p. 270 (1989)

[6] Borg G.G., Dalla Piazza S, Martin Y. et al. Proc. of the 16th European Conf. on Contr. Fus. and Plas. Phys. Venice Vol. 13 p. 1199 (1989)

[7] Borg G.G., Lister J.B. et. al. in preparation for submission to Nuc. Fus.

[8] Weisen H., Appert K., Borg G.G. et al. Phys. Rev. Lett. **63** p. 2476 (1989)

[9] Hasegawa A. and Chen L. Phys. rev. Lett. **35** p. 370 (1975)

[10] Hasegawa A. and Chen L. Phys. Fluids **19** p. 1924 (1976)

[11] Ross D.W., Chen G.L. and Mahajan S. Phys. Fluids **25** p. 652 (1982)

[12] Van Nieuwenhove R., Van Oost G., Noterdaeme J.-M, et al. Nuc. Fus. **28** p. 1603 (1988)

[13] Skiff F., Ono M. and Wong K.L. Phys. Fluids **27** p. 5 (1984)

[14] Ballico M.J., Brennan M.H., Cross R.C. et. al. Plas. Phys. and Contr. Fus. **30**, p1331 (1988)

[15] Borg G.G. and Cross R.C. Plas. Phys. and Contr. Fus. **29** p. 681 (1987)

[16] Koch R., Descamps F., Durodie F. et al. '*Study of the Coupling and Edge Effects during ICRF Heating Experiments using an Electrostatic Antenna on TEXTOR* IAEA technical meeting on ICRH/Edge physics Garching (1989)

[17] Collins GA., Lister J.B., Hofmann F. and Pochelon A. Private communication.

[18] Bures M., Jacquinot J., Start D. and Brambilla M. Nuc. Fus. **30** p. 251 (1990)

[19] Murphy A.B. Plas. Phys. and Contr. Fus. **31** p. 21 (1989)

[20] Lietti A. and Besson G. J. Phys. E. Sci. Instrum. **19** p. 557 (1986)

[21] Hoffmann D.J., Becraft W.R., Baity F.W. et al. Fus. Tech. **8** p. 392 (1985)

[22] Faulconer D.W. J. App. Phys. **54** p. 3810 (1983)

[23] Howatson A.M. 'An Introduction to Gas Discharges' Pergamon Press (1976)

(24) Joye B., Lietti A., Lister J.B. et al. Phys. Rev. Lett. **56** p. 2481 (1986)

[25] De Chambrier A., Duval B.P., Lister J.B. et al. Plas. Phys. and Contr. Fus. **31** p. 527 (1989)

[26] Appert K., Besson G., Borg G.G. et. al. Proc. of the Joint Int. Conf. on Plas. Phys., Kiev, invited paper (1987)

[27] Dudok de Wit Th., Duval B.P., Hollenstein Ch. and Joye B. Proc. of the 17th European Conf. on Contr. Fusion and Plasma Heating, Amsterdam Vol. 14 p. 1476 (1990)

FIGURE CAPTIONS

Fig. 1. TCA antenna and Rogowski configurations for a) symmetric excitation and b) asymmetric excitation. The arrows in each case indicate the direction of current flow to the antenna at any instant of time.

Fig. 2 a) Traces in the left column for asymmetric excitation show from top to bottom the simulated antenna current from equation (3) based on $\pm V_{int}/2$ at P and Q in Fig. 1, the I_f corresponding to V_{int} for half the antenna bar and the simulation of the fault current for symmetric excitation. In the right column are two experimental fault current traces for m=0 and m=1 excitation. A typical antenna currrent is shown in the top trace.

b) A full set of traces for asymmetric excitation.

c) The asymmetric rms fault current (I_f) amplitude plotted as a function of rms V_{int}.

Fig. 3 a) Measured minimum and maximum fault current loading and total loading vs antenna current for asymmetric excitation.

b) Simulated maximum fault current loading and total loading for symmetric excitation.

c) Traces showing from top to bottom the antenna current, total antenna loading, the fundamental and first harmonic components of the fault current and b_θ for symmetric excitation at 2.5 MHz during a sweep of the (2,1) DAW.

Fig. 4 Antenna loading traces versus total power for m = 1 excitation and two plasma densities. The results were taken with four types of side screen; solid metallic side screens, slit side screens, quartz side screens and side skirts protecting the antenna radial feeders.

Fig. 5 Apparatus used to test the properties of electrostatic screens.
a) Single bar antenna element fed symmetrically from below an earth plane.
b) The movable probe which measures $E_{||}$ by the potential difference between parallel metal strips.

Fig. 6 Plot of $E_{||}$ vs distance in the toroidal direction from the antenna element.

Fig. 7 Schematic diagram of the electrostatic screens.
a)Top view showing the 11 screen blades. The antenna bars are shown as dotted lines. The side screens are also shown.
b)View along the toroidal direction. The side screen, not shown, completely blocks the view down to a=195 mm. The plates supporting the blades were made of stainless steel in the case of earthed screens and ceramic in the case of floating screens. The antenna is shown dotted.

Fig. 8 Experimental arrangement showing the location of the screened and unscreened antennas in TCA.

Fig. 9 The edge plasma response to AWH.
a) Unshielded antennas (3,7).
b) Antennas (1,5) with earthed shields.

Fig. 10 Plasma global response to AWH.
a) Excitation by unshielded antennas (3,7).
b) Excitation by antennas (1,5) with earthed shields.
c) Excitation by antennas (2,6) with floating shields.
d)Without AWH.

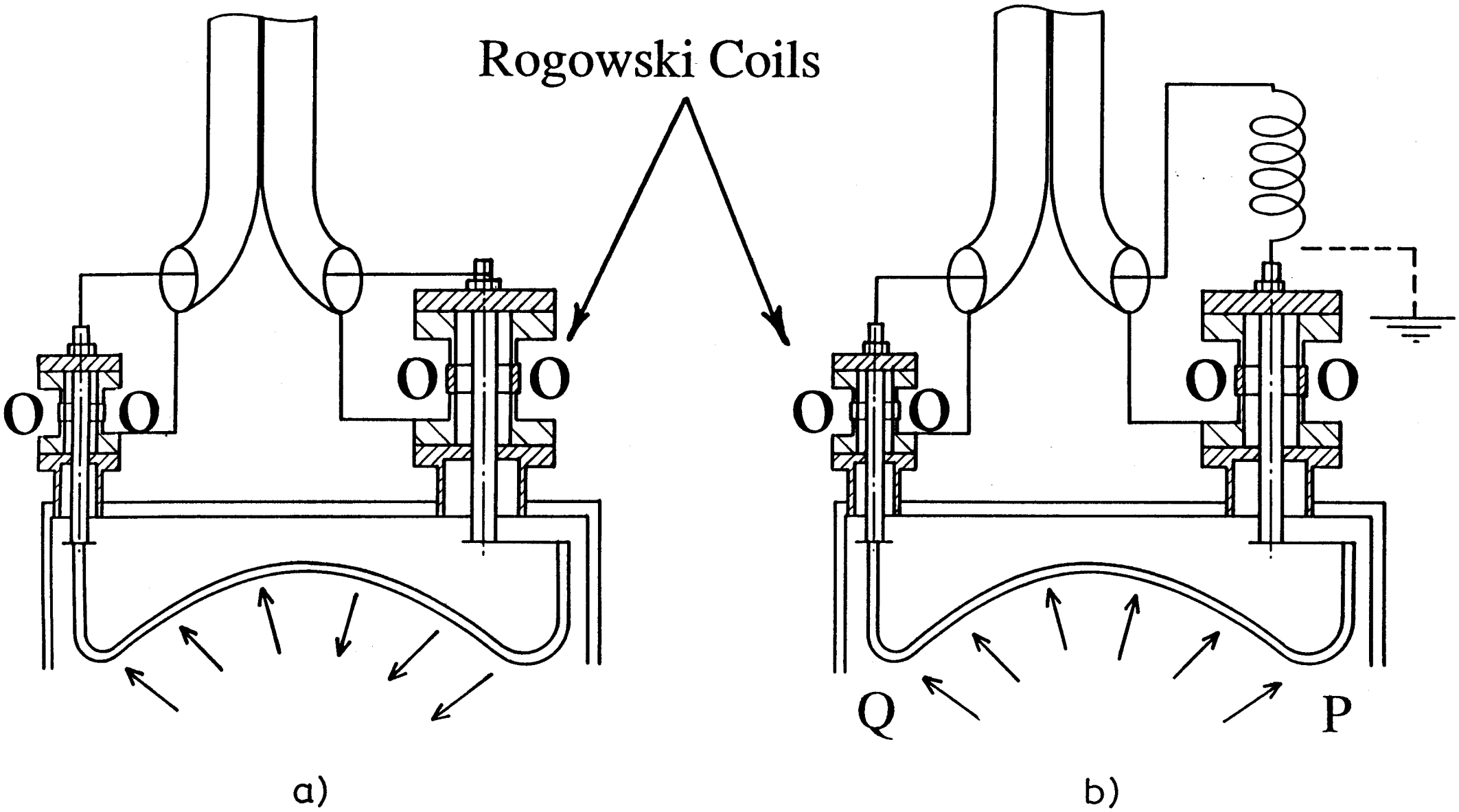

Fig. 1

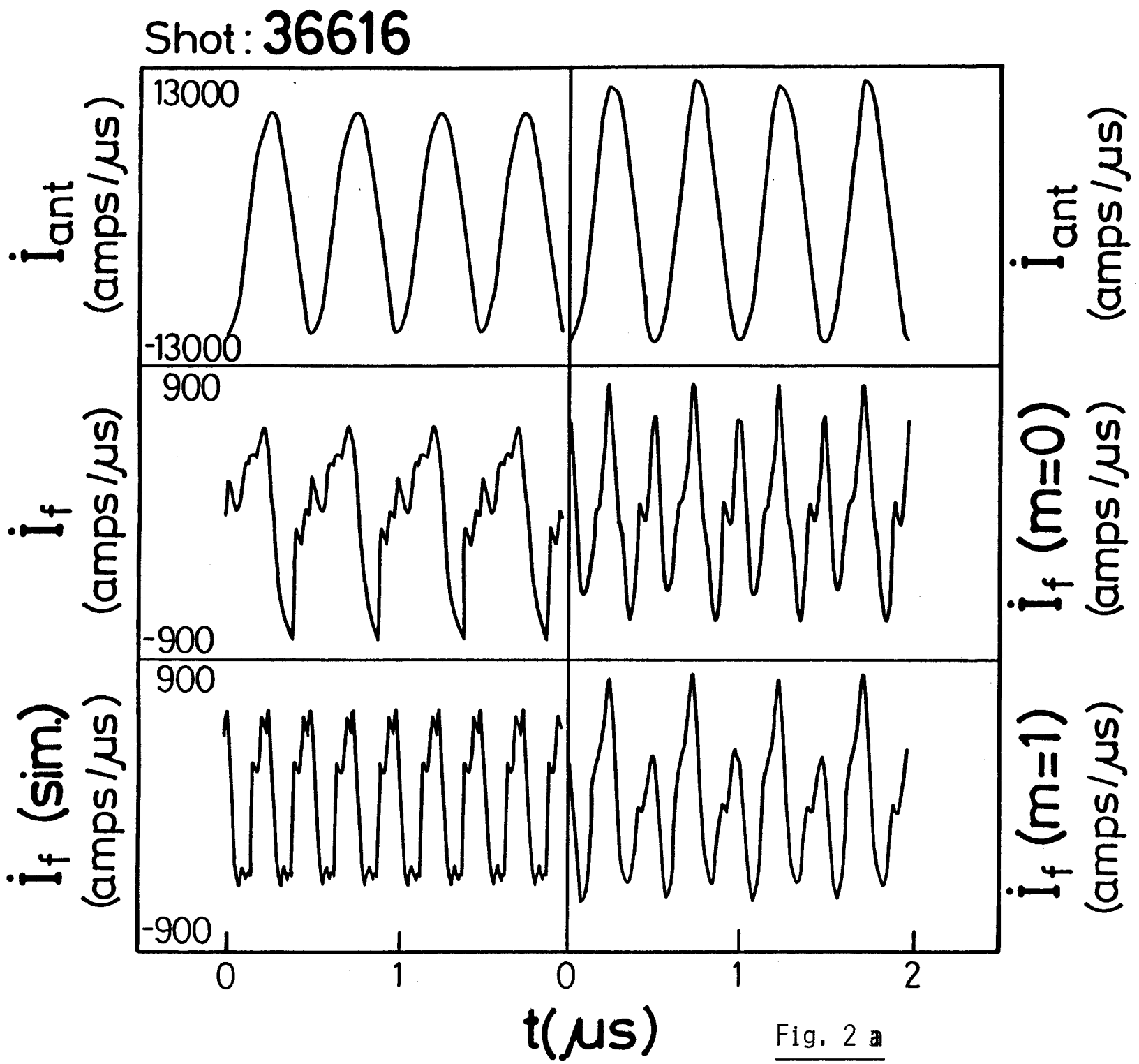
Shot: 36616
13000
-13000
i_{ant} (amps/μs)
900
-900
i_f (amps/μs)
900
-900
i_f (sim.) (amps/μs)
i_{ant} (amps/μs)
i_f (m=0) (amps/μs)
i_f (m=1) (amps/μs)
0
1
0
1
2
t(μs)

Fig. 2 a

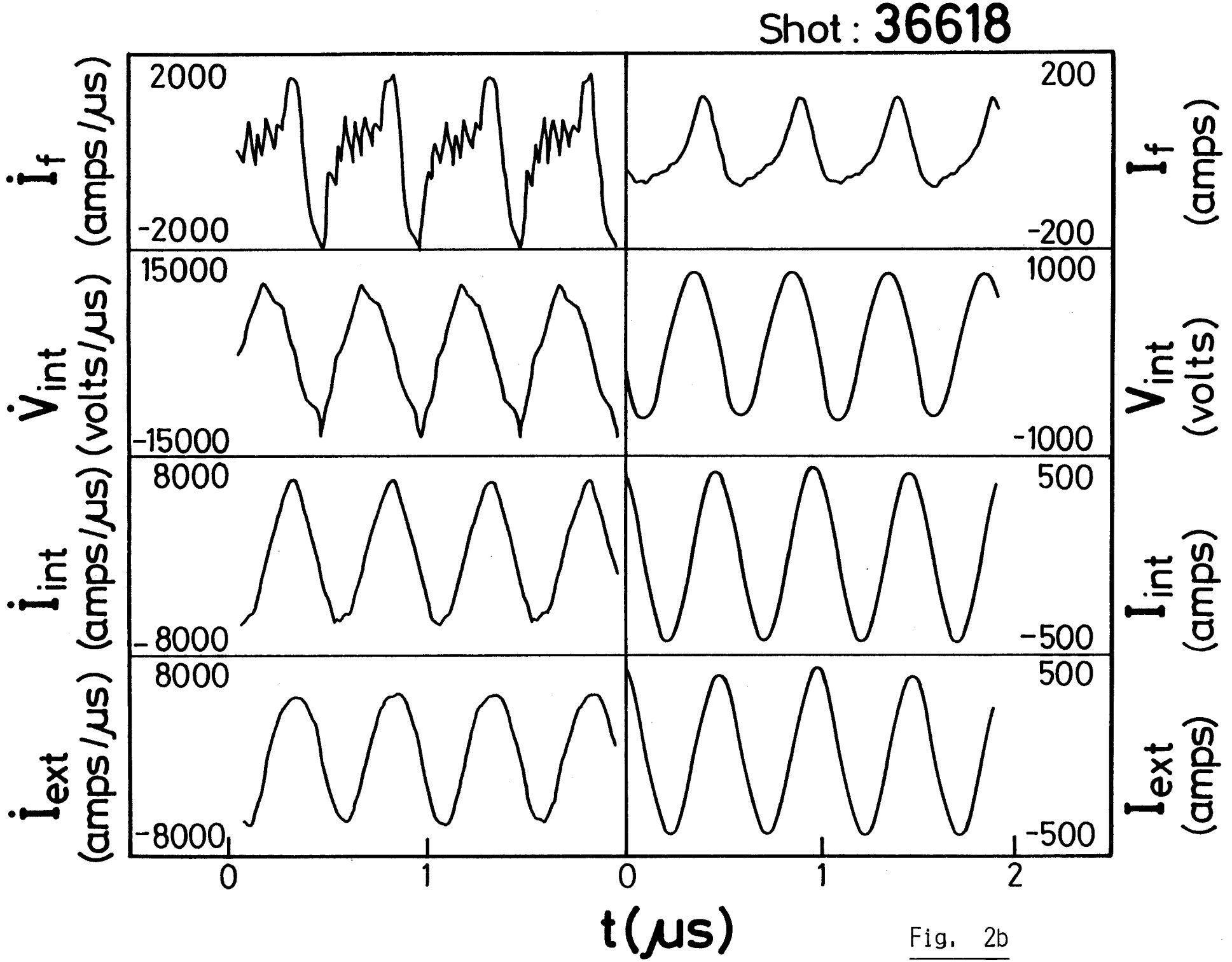
Shot : 36618
$\dot{I}_f$ (amps/μs)
2000
-2000
I_f (amps)
200
-200
$\dot{V}_{int}$ (volts/μs)
15000
-15000
V_{int} (volts)
1000
-1000
$\dot{I}_{int}$ (amps/μs)
8000
-8000
I_{int} (amps)
500
-500
$\dot{I}_{ext}$ (amps/μs)
8000
-8000
I_{ext} (amps)
500
-500
0
1
0
1
2
t(μs)

Fig. 2b

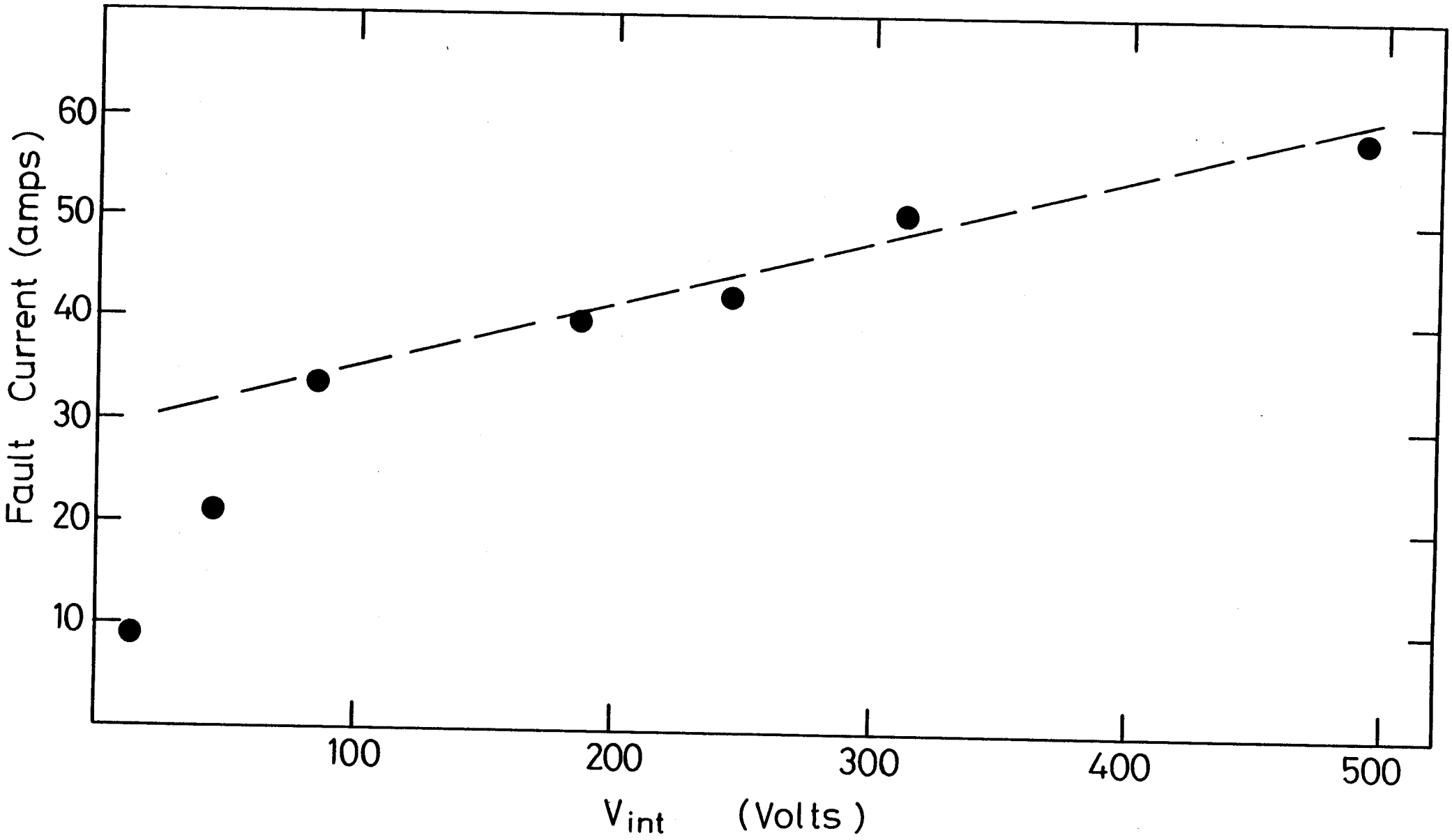
Fault Current (amps)
60
50
40
30
20
10
100
200
300
400
500
V_{int} (Volts)

Fig. 2c

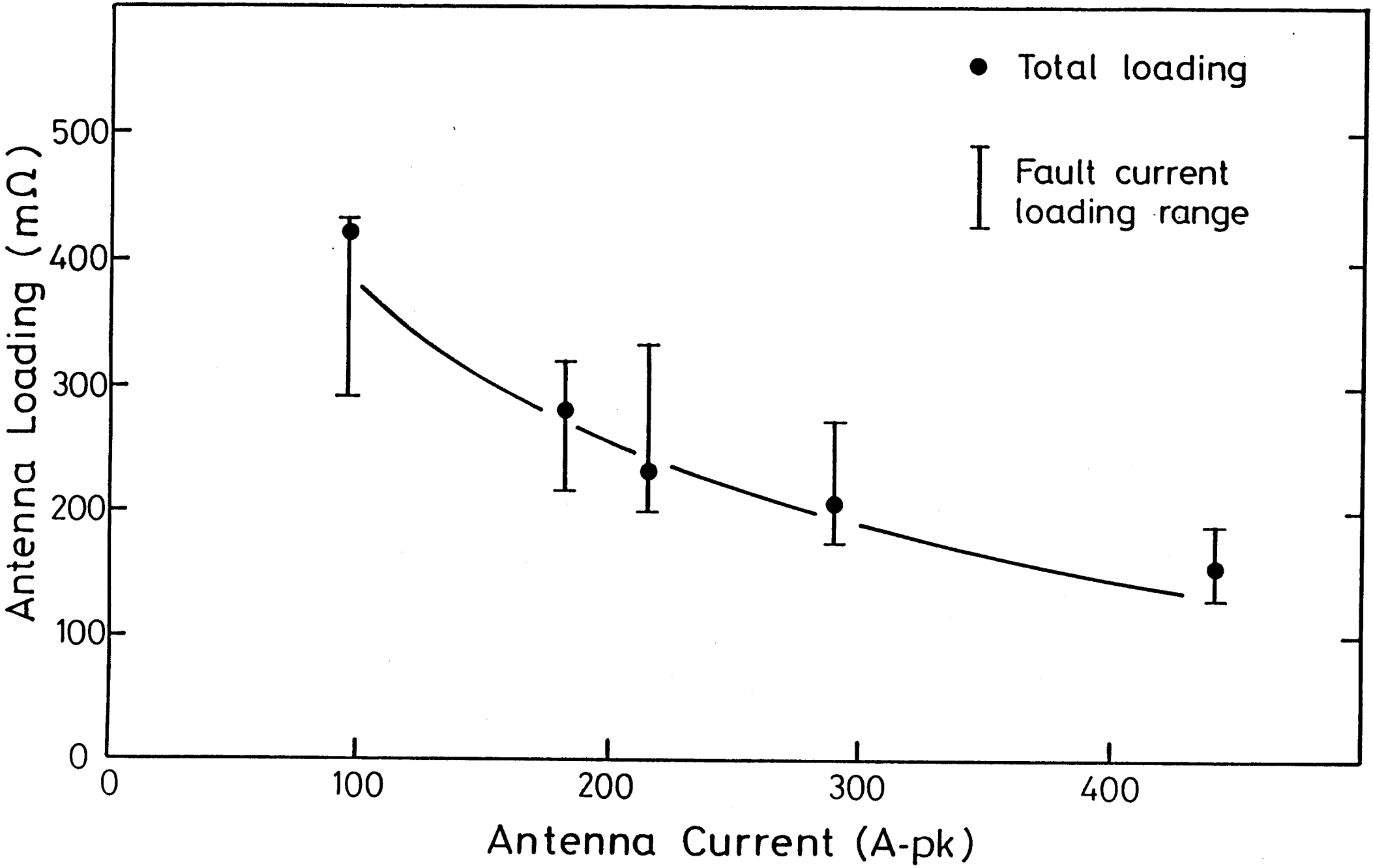
Total loading
Fault current loading range
Antenna Loading (mΩ)
500
400
300
200
100
0
0
100
200
300
400
Antenna Current (A-pk)

Fig. 3a

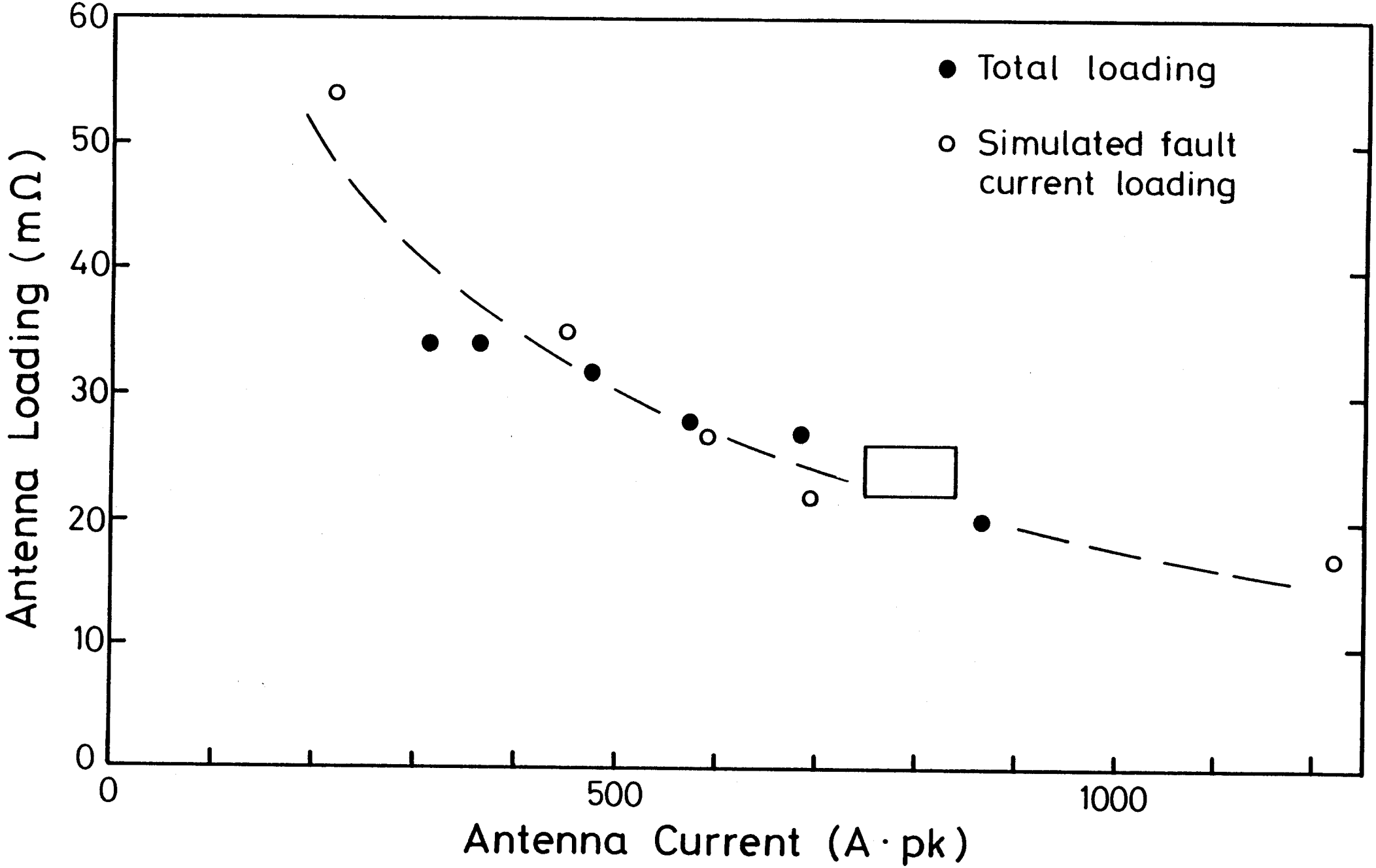
60
50
40
30
20
10
0
0
500
1000
Antenna Loading (mΩ)
Antenna Current (A·pk)
Total loading
Simulated fault current loading

Fig. 3b

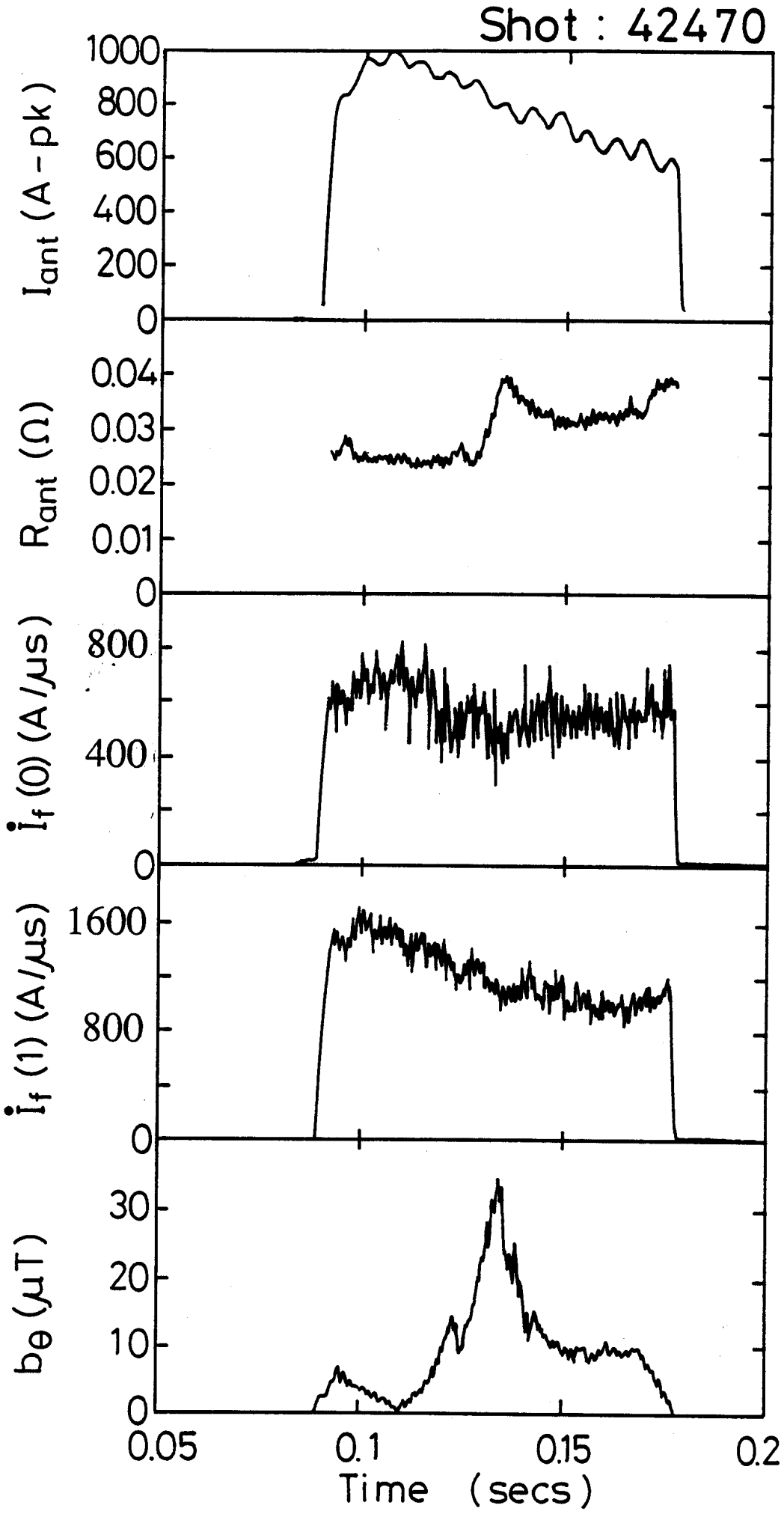
Shot : 42470
I_{ant} (A-pk)
1000
800
600
400
200
0
R_{ant} (Ω)
0.04
0.03
0.02
0.01
0
$\dot{I}_f$ (0) (A/μs)
800
400
0
$\dot{I}_f$ (1) (A/μs)
1600
800
0
b_θ (μT)
30
20
10
0
0.05
0.1
0.15
0.2
Time (secs)

Fig. 3c

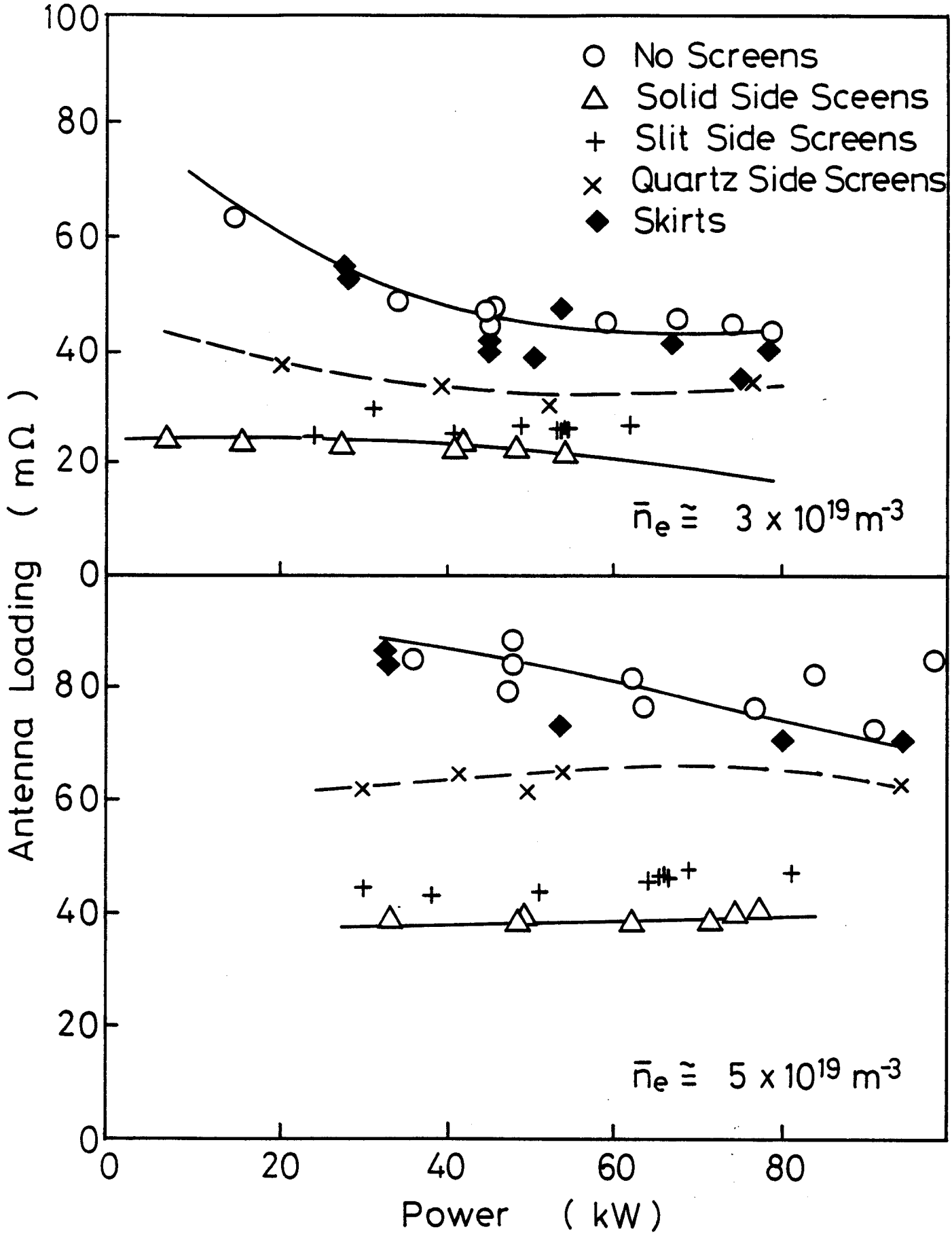
No Screens
Solid Side Sceens
Slit Side Screens
Quartz Side Screens
Skirts
$\bar{n}_e \cong 3 \times 10^{19} m^{-3}$
$\bar{n}_e \cong 5 \times 10^{19} m^{-3}$
Antenna Loading (mΩ)
Power (kW)
0
20
40
60
80
100

Fig. 4

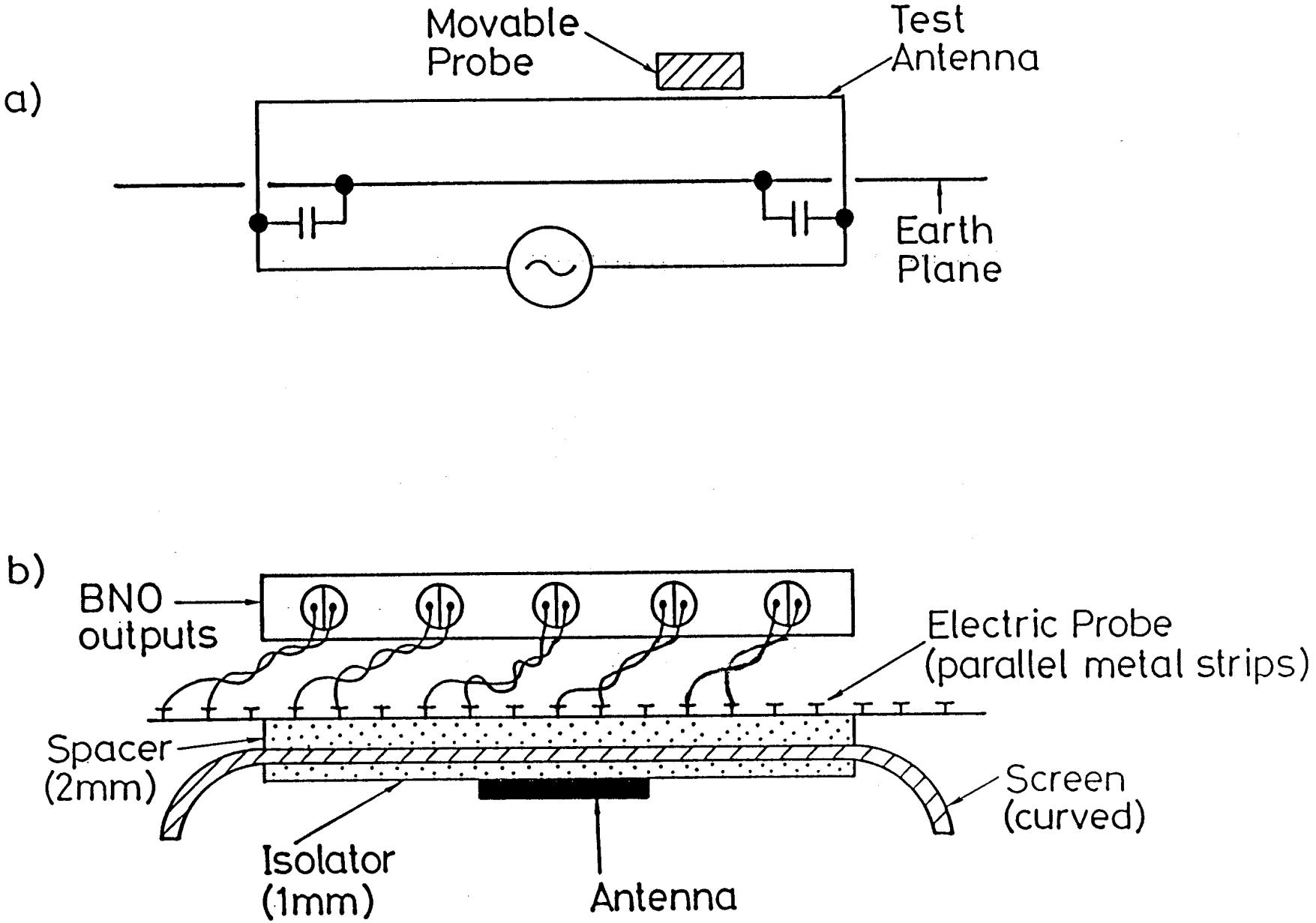
a)
Movable
Probe
Test
Antenna
Earth
Plane
b)
BNO
outputs
Electric Probe
(parallel metal strips)
Spacer
(2mm)
Screen
(curved)
Isolator
(1mm)
Antenna

Fig. 5

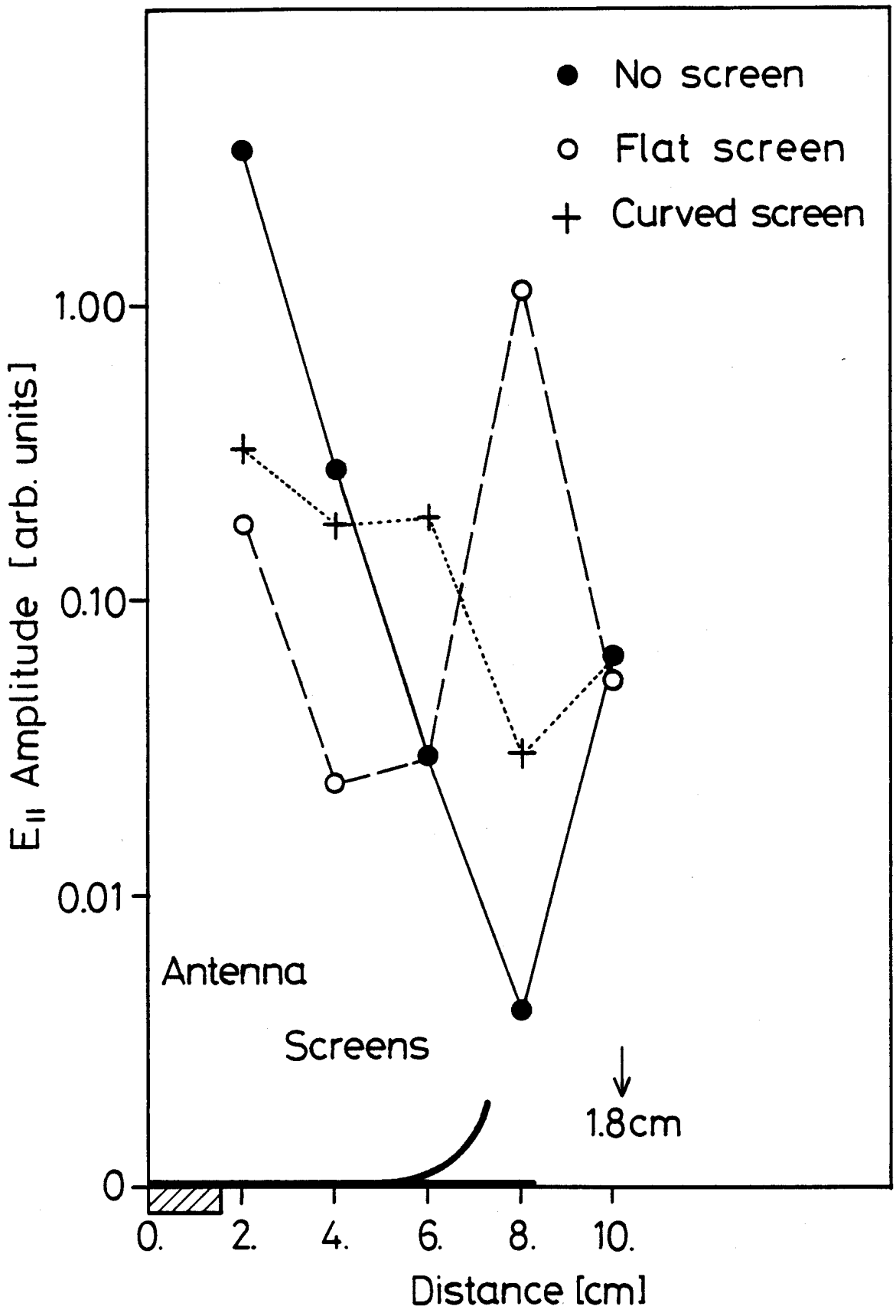
No screen
Flat screen
Curved screen
1.00
0.10
0.01
0
E_{II} Amplitude [arb. units]
Antenna
Screens
1.8cm
0.
2.
4.
6.
8.
10.
Distance [cm]

Fig. 6

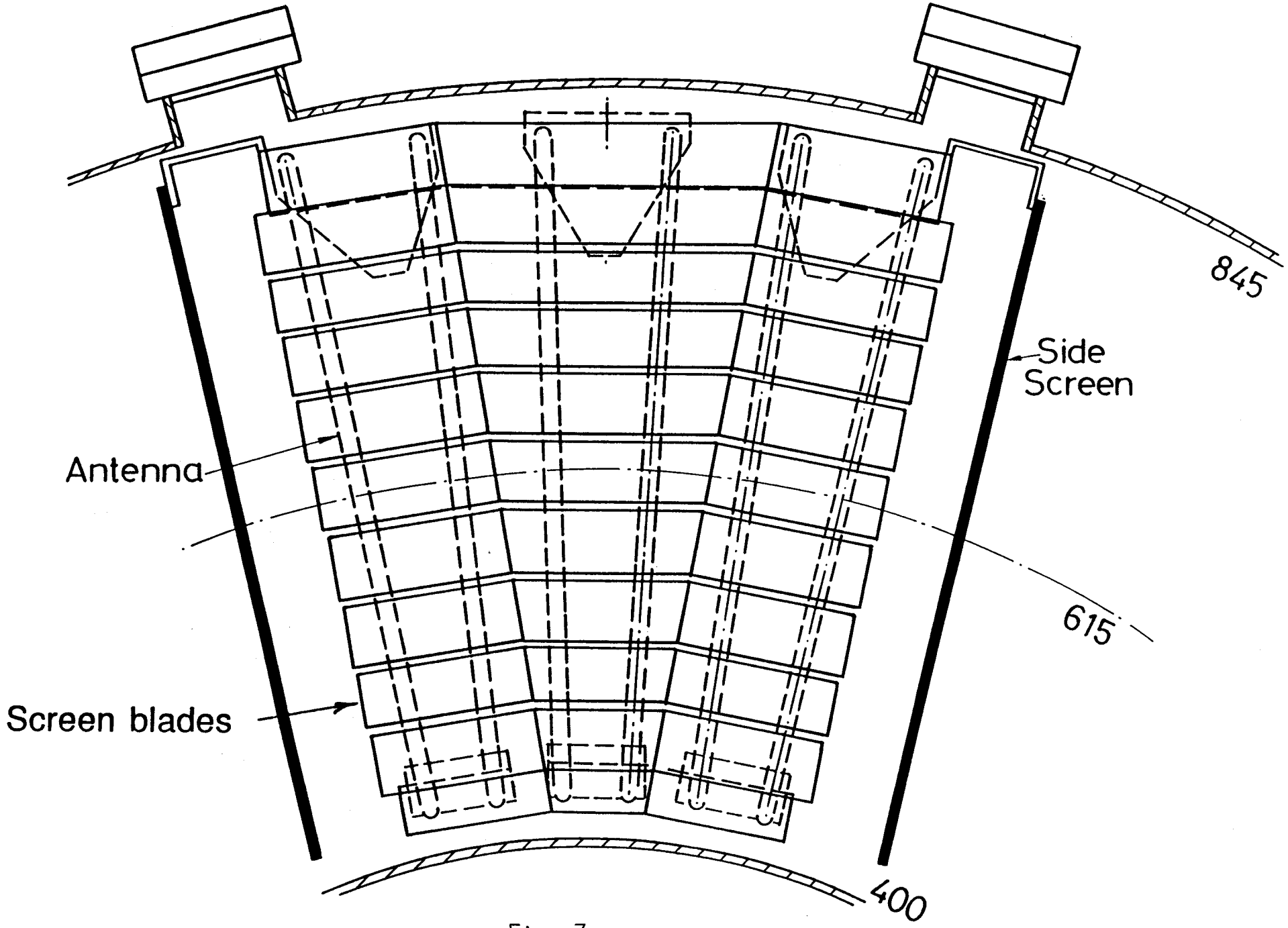

Fig. 7a

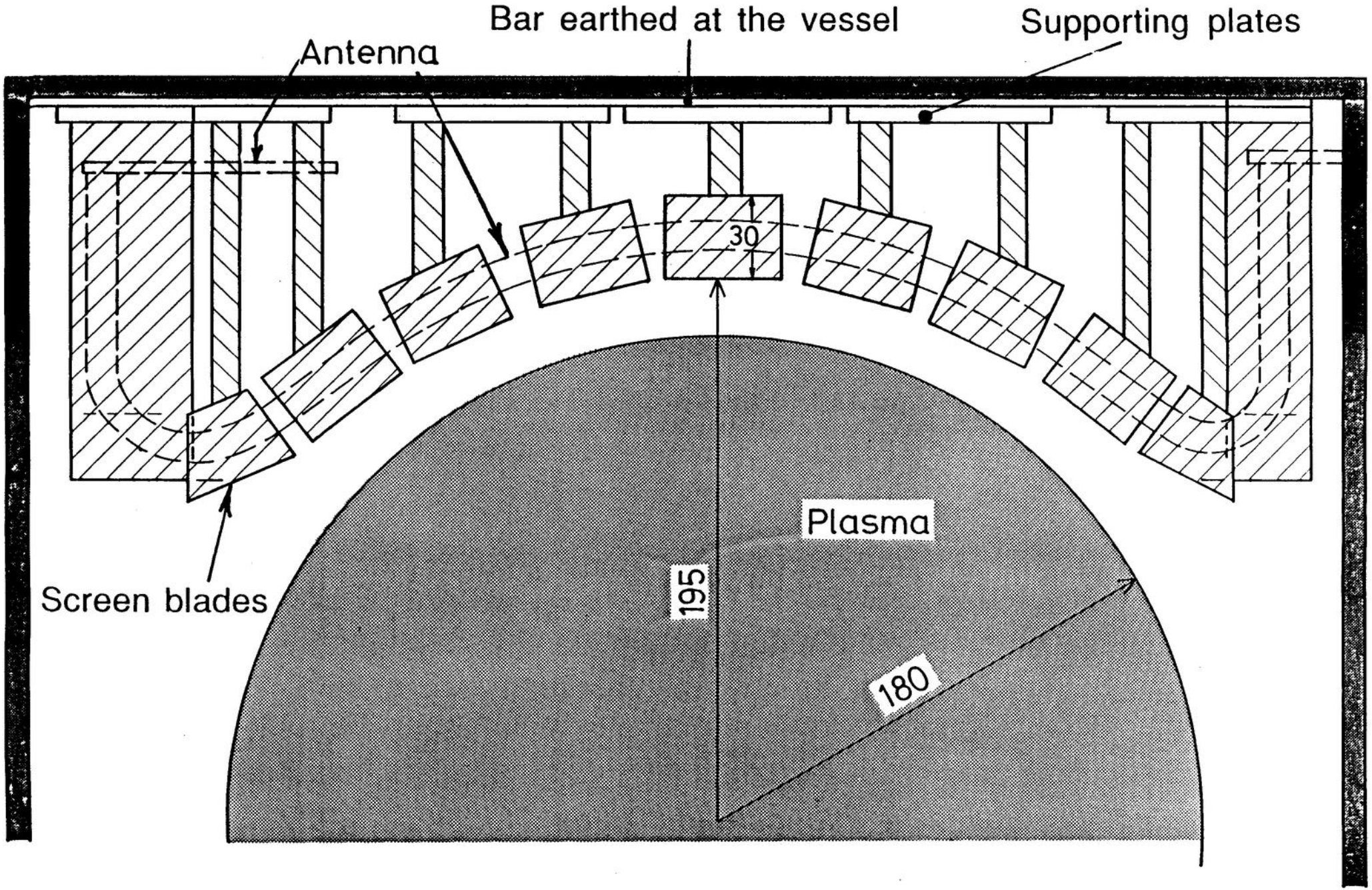
Bar earthed at the vessel
Supporting plates
Antenna
30
Plasma
195
180
Screen blades

Fig. 7b

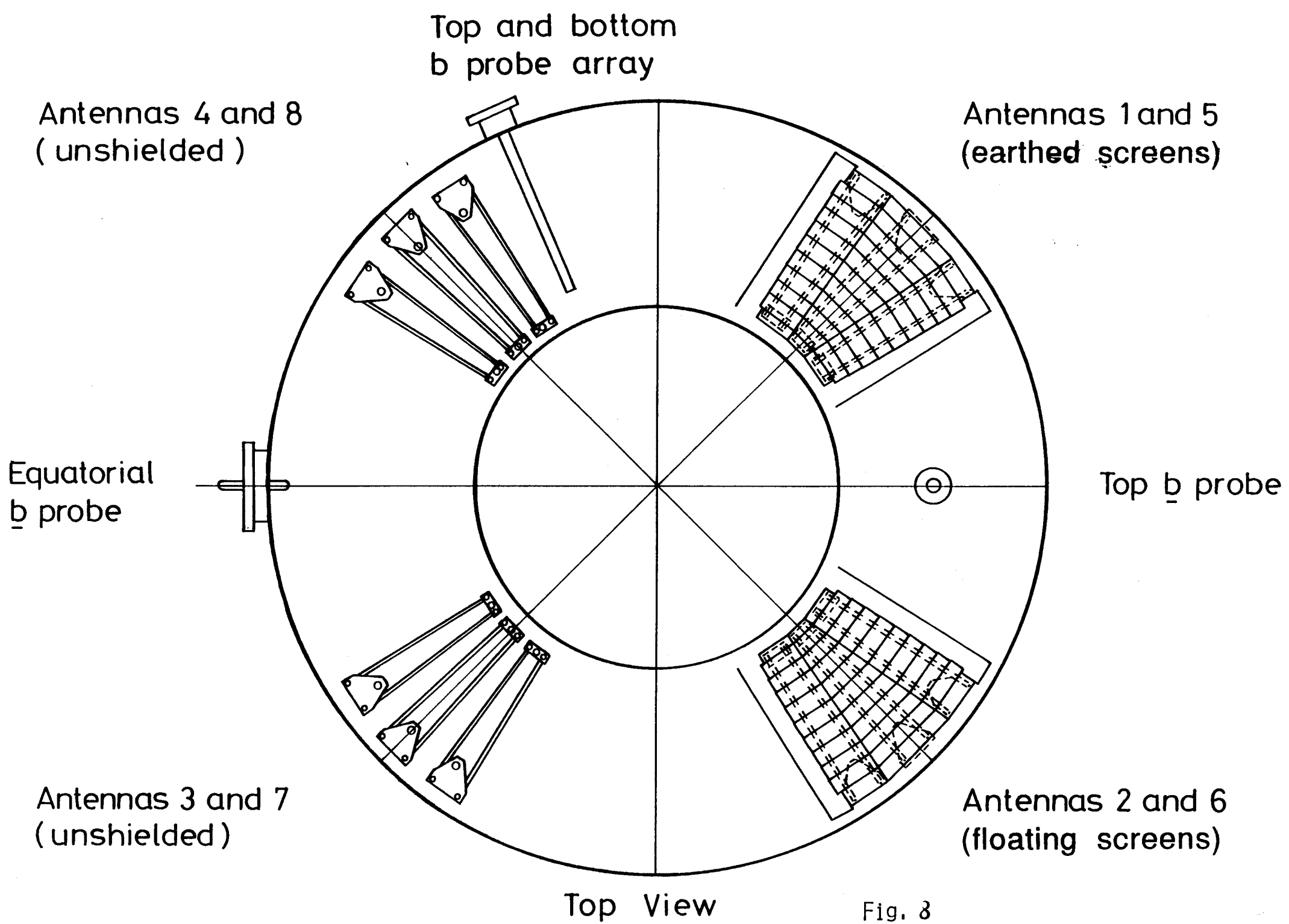
Top and bottom
b probe array
Antennas 4 and 8
(unshielded)
Antennas 1 and 5
(earthed screens)
Equatorial
b probe
Top b probe
Antennas 3 and 7
(unshielded)
Antennas 2 and 6
(floating screens)
Top View

Fig. 8

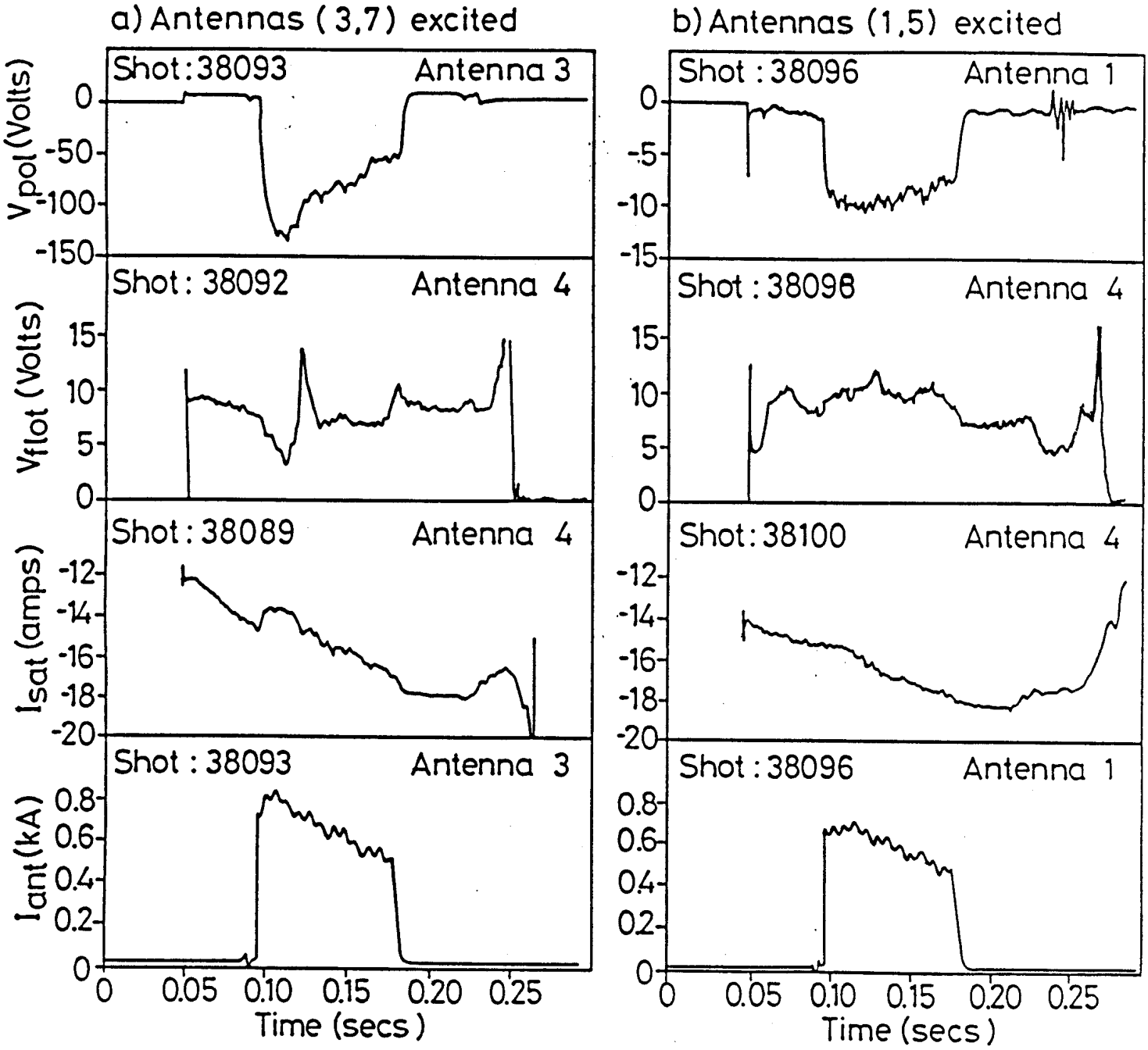
a) Antennas (3,7) excited
b) Antennas (1,5) excited
Shot:38093
Antenna 3
Shot : 38096
Antenna 1
Shot : 38092
Antenna 4
Shot : 38098
Antenna 4
Shot: 38089
Antenna 4
Shot: 38100
Antenna 4
Shot : 38093
Antenna 3
Shot : 38096
Antenna 1
V pol (Volts)
V flot (Volts)
I sat (amps)
I ant (kA)
Time (secs)
Time (secs)

Fig. 9

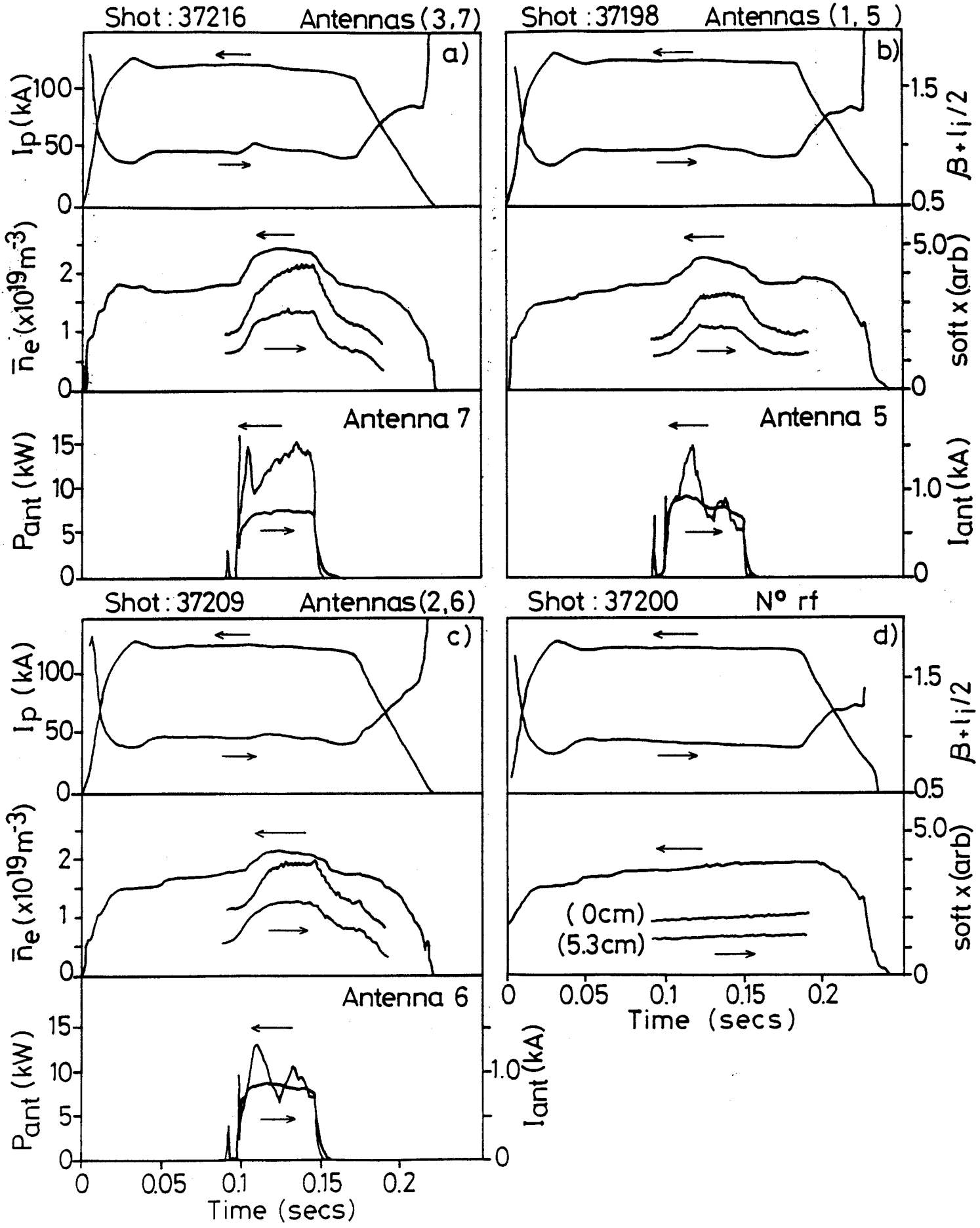
Shot : 37216
Antennas (3,7)
a)
Shot : 37198
Antennas (1, 5)
b)
Shot : 37209
Antennas (2,6)
c)
Shot : 37200
N° rf
d)
Ip (kA)
$\bar{n}_e$ (x10^{19}m^{-3})
P_{ant} (kW)
I_{ant} (kA)
$\beta + l_i/2$
soft x (arb)
Antenna 7
Antenna 5
Antenna 6
(0cm)
(5.3cm)
Time (secs)

Fig. 10